

# Liana Attachment to Supports Leads to Profound Changes in Xylem Anatomy and Cambium and Differentiating Xylem Transcriptional Profile

André Carvalho Lima<sup>1</sup>, Sónia Cristina da Silva Andrade<sup>1</sup>, Caian Souza Gerolamo<sup>1</sup>, Diego Souza<sup>1</sup>, Luiz Lehmann Coutinho<sup>2</sup>, Magdalena Rossi<sup>1</sup>, and Veronica Angyalossy<sup>1</sup>

<sup>1</sup>Universidade de Sao Paulo Instituto de Biociencias

<sup>2</sup>Universidade de Sao Paulo Escola Superior de Agricultura Luiz de Queiroz

August 29, 2023

## Abstract

Wood serves crucial functions in plants, yet our understanding of the molecular regulation governing the composition, arrangement, and dimensions of its cells remains limited. The abrupt change in wood anatomy of lianas represents an excellent model to address the underlying mechanism, although consistent triggering factors for this process remain uncertain. In this study we examined how physical support attachment impacts the development of lianescent xylem anatomy in *Bignonia magnifica* (Bignoniaceae), employing a comprehensive approach integrating detailed anatomical analysis with gene expression profiling of cambium and differentiating xylem. Our findings demonstrate that attachment to physical supports triggers the formation of lianescent xylem, leading to increased vessel size, range of vessel sizes, broader vessel distribution, reduced fiber content, and higher potential specific water conductivity. These shifts in wood anatomy coincide with the downregulation of genes associated with cell division and cell wall biosynthesis, and the upregulation of transcription factors (TFs), defense/cell death, and hormone-responsive genes in the lianescent xylem. Based on our results, we propose a model delineating the molecular control underlying the formation of lianescent xylem, revealing how the increased complexity of lianescent anatomy reflects a more intricate transcriptional regulatory network encompassing a more diverse repertoire of TFs and hormone-responsive genes.

## Liana Attachment to Supports Leads to Profound Changes in Xylem Anatomy and Cambium and Differentiating Xylem Transcriptional Profile

André Carvalho Lima<sup>1,2,\*</sup>, Sónia Cristina da Silva Andrade<sup>3</sup>, Caian Souza Gerolamo<sup>1</sup>, Diego Trindade de Souza<sup>1</sup>, Luiz Lehmann Coutinho<sup>4</sup>, Maria Magdalena Rossi<sup>1</sup>, Veronica Angyalossy<sup>1</sup>

<sup>1</sup> Departamento de Botânica, Instituto de Biociências, Universidade de São Paulo, São Paulo, Brazil. <sup>2</sup>Present address: Faculdade de Ciências Agronômicas, Universidade Estadual Paulista, Botucatu, Brazil. <sup>3</sup> Departamento de Genética e Biologia Evolutiva, Instituto de Biociências, Universidade de São Paulo, São Paulo, Brazil. <sup>4</sup> Departamento de Zootecnia, Escola Superior de Agricultura 'Luiz de Queiroz' (ESALQ), Universidade de São Paulo, Piracicaba, Brazil.

\*Corresponding author: André C Lima - [andrec.lima@gmail.com](mailto:andrec.lima@gmail.com)

## ORCIDs

André C Lima: 0000-0001-9183-3064

Sónia CS Andrade: 0000-0002-1302-5261

Caian S Gerolamo: 0000-0003-1819-5371

Diego T de Souza: 0000-0001-8783-2333

Luiz L Countinho: 0000-0002-7266-8881

Magdalena Rossi: 0000-0003-3650-772X

Veronica Angyalossy:0000-0002-9823-9946

## Summary

Wood serves crucial functions in plants, yet our understanding of the molecular regulation governing the composition, arrangement, and dimensions of its cells remains limited. The abrupt change in wood anatomy of lianas represents an excellent model to address the underlying mechanism, although consistent triggering factors for this process remain uncertain. In this study we examined how physical support attachment impacts the development of lianescent xylem anatomy in *Bignonia magnifica* (Bignoniaceae), employing a comprehensive approach integrating detailed anatomical analysis with gene expression profiling of cambium and differentiating xylem. Our findings demonstrate that attachment to physical supports triggers the formation of lianescent xylem, leading to increased vessel size, range of vessel sizes, broader vessel distribution, reduced fiber content, and higher potential specific water conductivity. These shifts in wood anatomy coincide with the downregulation of genes associated with cell division and cell wall biosynthesis, and the upregulation of transcription factors (TFs), defense/cell death, and hormone-responsive genes in the lianescent xylem. Based on our results, we propose a model delineating the molecular control underlying the formation of lianescent xylem, revealing how the increased complexity of lianescent anatomy reflects a more intricate transcriptional regulatory network encompassing a more diverse repertoire of TFs and hormone-responsive genes.

**Keywords:** gene expression profile; lianas; transcriptome; wood; wood traits; secondary xylem; differentiation.

## Introduction

Wood serves three essential functions in plants: providing mechanical support, positioning leaves and reproductive organs for photosynthesis and pollination/dispersion; conducting water and nutrients; and storing water and nutrients (Baas *et al.*, 2004). The evolution of cellular specialization in Angiosperm wood, or secondary xylem, has led to a division of labor among different cell types. Fibers primarily provide mechanical support, vessels conduct water and minerals, and axial and radial parenchyma store resources (Tyree & Zimmermann, 2002). Secondary xylem formation occurs through the activity of the cambium, a lateral meristem, producing the different cell types of the secondary xylem toward the inside of the stem, and secondary phloem toward the exterior (Evert, 2006).

Studies on model species, like *Arabidopsis thaliana* and *Populus* have significantly advanced the understanding of cambium function and activity, and xylem differentiation (Groover, 2005; Robischon *et al.*, 2011; Ye & Zhong, 2015). Crucial molecular components, such as the *TDIF/CLE41/CLE44-TDR/PXY-WOX4* module controlling cambial maintenance and proliferation (Hirakawa *et al.*, 2010; Zhang *et al.*, 2019), and the secondary cell wall (SCW) biosynthesis master transcription factors NACs (*NST1*, *XND1*, *VND6*, *VND7*, and *SND1*) and MYBs (Kubo *et al.*, 2005; Zhong *et al.*, 2006, 2007; Zhang *et al.*, 2020), have been characterized in *A. thaliana*. These findings have proven to be conserved among diverse herbaceous and woody species (Hu *et al.*, 2010; Zhong *et al.*, 2011; Hirakawa & Bowman, 2015). However, our understanding of the molecular regulation underlying the cellular composition, arrangement, and dimensions of secondary xylem, crucial for wood functions, remains limited (Ziemińska *et al.*, 2015; Beckman, 2016).

Advancements in technologies, like high-throughput sequencing have enabled molecular studies in non-model species, revealing unique features and processes absent in model species organisms (Carpentier *et al.*, 2008; Wang *et al.*, 2009). Within this context, lianas exhibit a distinctive set of wood anatomical characteristics associated with high flexibility, conduction efficiency, and intraindividual plasticity in wood traits (Fig. 1). These attributes make lianas an excellent model for investigating vascular system differentiation. Despite evolving independently in various plant groups, most lianas share convergent secondary xylem anatomical

features, including reduced fibers, wide vessels (up to 500  $\mu\text{m}$  in diameter) associated with small vessels (referred to as vessel dimorphism by Carlquist, 1981), and the presence of soft tissues interspersed in the xylem (Schenck, 1893; Obaton, 1960; Carlquist, 1985). These common features are collectively known as the “lianescent vascular syndrome” (Angyalossy *et al.* , 2015).

Most lianas, however, show a dense fibrous xylem with small vessels, resembling the xylem of self-supporting species at the beginning of secondary development (Schenck, 1893; Obaton, 1960; Caballé, 1998). The transition from the formation of this dense xylem (termed as self-supporting xylem hereafter) to the development of that showing the lianescent vascular syndrome (termed as lianescent xylem hereafter) occurs abruptly, as seen in adult stem cross-sections (Fig. 1b). Importantly, self-supporting and lianescent xylems are produced simultaneously along liana stems. While older sections produce lianescent xylem, younger parts continue to form self-supporting xylem. Furthermore, recent findings indicate that attachment to supports triggers the production of lianescent xylem in the twining liana *Condylocarpon guianensis* (Soffiatti *et al.* , 2022). However, it remains unclear if this triggering factor is consistent across lianas from different lineages or with different climbing methods.

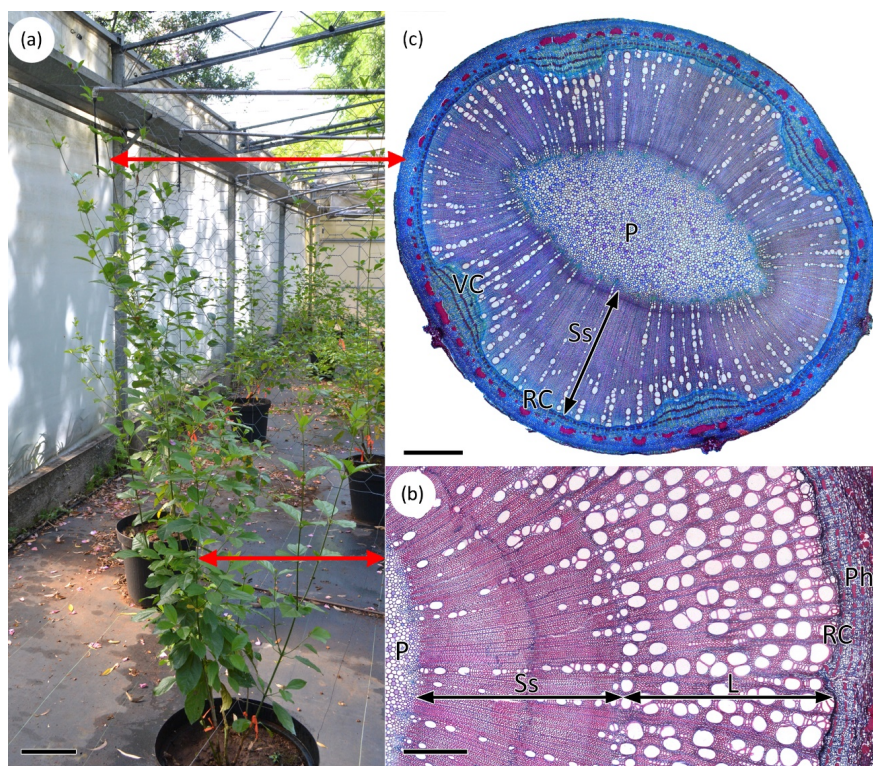


**Fig. 1.** *B. magnifica* wood plasticity seen in stem cross-sections along the stem. (a) A one-year-old plant grown with support. (b) Secondary xylem formed by the regular cambium (RC) in older portions of the stem shows an abrupt transition from the self-supporting xylem (Ss) formed at the beginning of development to the lianescent xylem (L). The lianescent xylem is characterized by the presence of wide vessels, which are associated with narrow vessels and fewer fibers. (c) The secondary xylem in younger portions of the stem is composed only of the self-supporting xylem (SS) formed by a high proportion of fibers and small vessels. It is possible to see the innermost position of the four regions of variant cambium (VC), responsible for the formation of phloem wedges characteristic of Bignoniaceae lianas, intercalated with the regular cambium (RC). Scales: (a) 33 cm, (b) 1 mm, (c), 500  $\mu\text{m}$ . P: pith; Ph: secondary phloem.

Here we tested the hypothesis that liana attachment to physical supports promotes the formation of lianes-

cent xylem by the cambium in older stem parts in the tendril climber *Bignonia magnifica* (Bignoniaceae). We propose that intraindividual plasticity in wood anatomy results from remodeling of the cambium and differentiating xylem transcriptome in these regions. By characterizing the anatomy of self-supporting and lianescent xylem, analyzing differential gene expression in the cambium and differentiating xylem, and providing a manually-curated comprehensive annotation, we propose a model for the molecular control of lianescent xylem differentiation. Our findings indicate distinct expression patterns between self-supporting and lianescent phases, with upregulation of cell division and cell wall-related transcripts in self-supporting xylem and a more intricate transcriptional regulation network, involving a diverse repertoire of transcription factors (TFs) and hormone-responsive genes.

## Material and Methods

### Plant Material

*Bignonia magnifica* W. Bull, Bignoniaceae, is native to Central America and northern South America (Lohmann & Taylor, 2014). It belongs to the monophyletic tribe Bignonieae, which is predominantly composed of lianas that climb using terminal leaflet-modified tendrils. Bignonieae is the most diverse and abundant clade of lianas in neotropical lowland forests (Gentry, 1986). A synapomorphy of the tribe is the presence of four or multiples of four, equidistant phloem wedges formed by variant regions of the cambium, which are located more internally in the stem due to its reduced xylem production (Lohmann & Taylor, 2014; Pace *et al.*, 2015; Fig. 1c).

### Growth Conditions

Clones of *Bignonia magnifica* were obtained from cuttings of a single plant cultivated at the gardens of the Biosciences Institute of the University of São Paulo, Brazil (23.56° S, 46.73° W). The average annual temperature in the region is 21.5°C and the mean total annual precipitation is approximately 1600 mm (Brazil National Weather Institute – [www.inmet.gov.br](http://www.inmet.gov.br)).

Sixteen one-year-old plants, each measuring one meter in height, were transplanted to pots measuring 60 cm in diameter and 50 cm in height with soil rich in organic matter in April 2016 (Fig. 2a). Six of these plants were grown with physical supports (stainless-steel wire meshes, 2.1 mm diameter wire, 7x7 cm mesh, Fig. 2b) for two years: five plants were used for self-supporting and lianescent secondary xylem anatomy analysis, and one plant was selected for the collection of cambium and differentiating xylem samples for transcriptome assembling and differential gene expression analysis. The remaining ten plants had their lateral branches and main stem apices pruned to stimulate the production of new branches of the same age (Fig. 2c). These ten plants were divided into two groups for the analysis of physical support impact on the lianescent xylem formation: one group was grown with physical supports (Fig. 2d), and the other group was grown without support aid (Fig. 2e). Pots were spaced 1.5 m apart and were watered to a maximum field capacity three times a week for the first year and weekly thereafter.

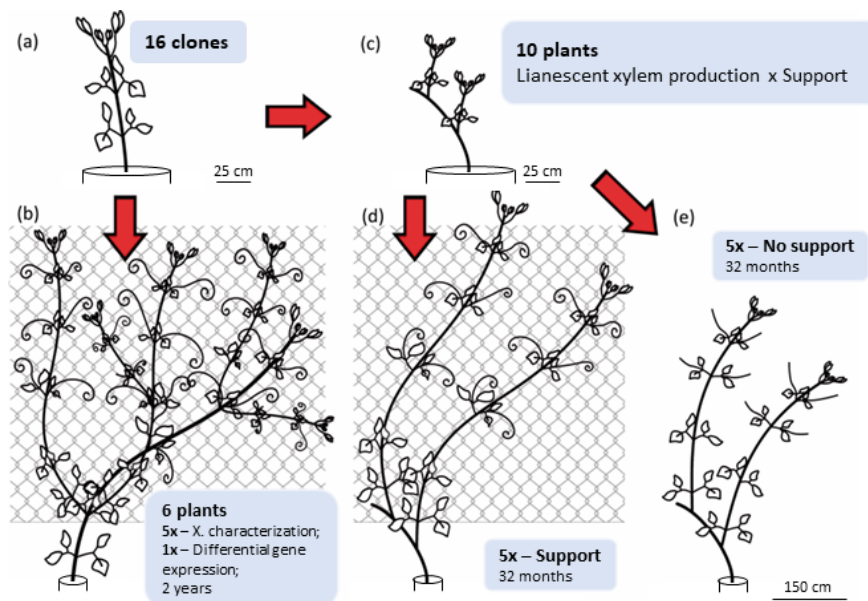


**Fig. 2.** Schematic diagram showing plant material and growth conditions. (a) Plant material consisted of 16 clones propagated through cuttings. (b) Six plants were grown besides physical supports (wire meshes) for two years: five plants were used for self-supporting and lianescent xylem (X.) anatomy characterization, carried at 4/5 of the distance from the shoot apex to the base, in the same cross-section; and one plant had the cambium and differentiating xylem sampled for transcriptome assembling and differential gene expression analysis. Tissue was sampled from 60 cm from the shoot apex (around the 10<sup>th</sup> internode) to the base of the stem (*ca.*20<sup>th</sup> internode). (c) Ten plants had lateral branches and main stem apices pruned to stimulate the production of new branches of the same age. They were grown for 32 months and were used to assess the relationship between lianescent xylem production and physical support attachment. (d) Five pruned plants were grown beside physical supports. (e) The other five pruned plants were grown without physical support. Scale bars: (a) and (c) 25 cm; (b), (d) and (e) 150 cm.

### Xylem Anatomy Analysis

To characterize self-supporting and lianescent xylem anatomy, we sampled the longest stems from the five unpruned plants (Fig. 2b after two years of cultivation, in May 2018). Due to differences in sampled stem lengths, which ranged from 3.6 to 8.4 m, self-supporting and lianescent xylems were characterized at 4/5 of the distance to the base, in the same cross-section. After collection, the samples were immediately fixed in FAA 50 (10% formalin, 5% acetic acid, 50% alcohol). Subsequently, the samples were rehydrated, embedded with polyethylene glycol 1500, and transversal and longitudinal sections from 8 to 15  $\mu$ m in thickness were made using a sliding microtome, as described by Barbosa *et al.*(2010). Additionally, portions of self-supporting and lianescent xylem were dissected under a stereomicroscope and macerated in Franklin's solution (Berlyn & Miksche, 1976).

Photomicrographs were captured using a Leica DML photomicroscope attached to a digital camera DFC 310FX, and measurements were performed using ImageJ v1.52a (Schneider *et al.* , 2012). Secondary xylem characterization was based on the IAWA List of Microscopic Features for Hardwood Identification (IAWA Committee, 1989) and Scholz *et al.* (2013). Secondary xylem characters were analyzed with a magnification of 200 $\times$  or 400 $\times$ , while the intervessel pit diameter was the only analyzed parameter requiring a higher magnification of 1,000 $\times$  under oil immersion. Relative areas of fibers, axial parenchyma, and rays were calculated by analyzing six 0.1 mm<sup>2</sup> images from random portions of the transverse section (Gerolamo & Angyalossy, 2017). The amount of xylem produced by the cambium was measured by calculating the average length of three straight lines from the cambium to the pith. The vessel grouping index was measured by the

ratio of total number of vessels to total number of vessel groupings, including solitary and grouped vessels (Scholz *et al.* 2013). The equivalent vessel diameter ( $D_v$ ;  $\mu\text{m}$ ) was calculated by measuring the vessel lumen area ( $A$ ;  $\mu\text{m}^2$ ) and using the formula:

$$D_v = (4A\pi^{-1})^{1/2}$$

The hydraulic diameter ( $D_h$ ), corresponding to the mean diameter that all sampled vessels would have to correspond to the total conductivity of the same number of vessels ( $n$ ) (Tyree *et al.* , 1994, Scholz *et al.* , 2013) was calculated using the formula:

$$D_h = (\sum_1^n D_v^4 n^{-1})^{1/4}$$

Potential specific conductivity ( $K_p$ ;  $\text{kg m}^{-1} \text{Mpa}^{-1} \text{s}^{-1}$ ) was calculated following Poorter *et al.* (2010) using the formula:

$$K_p = (\pi \rho_w 128 \eta^{-1}) V_d D_v^4$$

where  $D_h$  (m) is the vessel hydraulic diameter,  $\rho_w$  is water density at 20 °C ( $998.2 \text{ kg}\cdot\text{m}^{-3}$ ),  $\eta$  is the viscosity index of water ( $1.002 \times 10^{-9} \text{ MPa s}^{-1}$  at 20°C), and  $V_d$  is vessel density ( $\text{m}^{-2}$ ). Sample sizes were recommended by Scholz *et al.* (2013). Data normality and variance homogeneity were tested using Shapiro-Wilk and Levene’s tests, respectively. To compare each self-supporting and lianescent xylem anatomy characteristics, the Student’s t-test for parametric data, and the Mann-Whitney test for nonparametric data were applied in R software v.3.6.1 (R Core Team, 2014).

### Effect of Support on Lianescent Xylem Formation

To investigate the impact of support availability on the formation of lianescent xylem, we analyzed plants cultivated for 32 months, both with and without support (Fig. 2d and 2e, respectively). Two-centimeter-length stem samples were collected at regular 50 cm intervals, starting from the apex and avoiding nodes and potential injury. Subsequently, fresh cross-sections 10 to 25  $\mu\text{m}$  in thickness were obtained using a sliding microtome. Sections were then mounted unstained on 50% glycerin semi-permanent slides, or double stained with 1% Astra Blue and 1% Safranin (Bukatsch, 1972). Photomicrographs were captured as previously described.

### Samples for Differential Expression Analysis

To comprehend the transcriptional control mechanism responsible for the concomitant formation of the self-supporting and lianescent xylem in different portions of the same plant of *B. magnifica* , we sampled the cambium and differentiating xylem of entire internodes samples (approximately 30 cm long) collected from 60 cm from the shoot apex to the base of the stem (from around the 10<sup>th</sup> to the 20<sup>th</sup> internodes), along different stems of a single plant. After two years of cultivation, the sampling was conducted in April 2018 during the period of active cambium by peeling the bark and gently scraping the exposed xylem (Allona *et al.* , 1998; Sterky *et al.* , 1998; Perry *et al.* , 2021). The cambial activity was assessed by anatomical analysis (Supporting Information Fig. S1) and the ease with which the bark was peeled (Wilcox, 1962; Melder *et al.* , 2015). We chose this sampling strategy to avoid that the observed differences could be a product of, or be masked by, allelic variations, as *B. magnifica* is a wild, highly heterozygous species with no available sequence data. Given our focus on cambium and differentiating xylem, we also avoided sampling tissues below the peeled bark to prevent collecting other tissues, such as phloem and cortex, as the bark in the species was fragile and wrapped immediately after removal. This also prevented sampling the cambium and phloem from the phloem wedges (Supporting Information Fig. S2), what would add complexity to our analysis and was out of the scope of the present work. The innermost position of the variant cambium in the stem facilitated the collection of only regular portions for differential expression analysis, which were the only ones analyzed for this purpose. Tissues were immediately frozen in liquid nitrogen and stored at -80 °C. Before tissue harvest, each stem segment had its base cut and stored in 50 % alcohol to determine the xylem phase, self-supporting or lianescent, and any segment showing dubious or transitional anatomy,

and the segment next to it were discarded. Six pools of self-supporting and six pools of lianescent cambium and differentiating xylem, composed of 8-19 segments each, were collected for sequencing and differential expression analysis.

## RNA Extraction, Library Construction, and Sequencing

We extracted total RNA from the collected samples after sample lyophilization using ReliaPrep™ RNA Tissue Miniprep System (Promega Corporation) following manufacturer protocol. The quantity and quality of the extracted RNA were assessed using a Qubit (Thermo Scientific), while RNA integrity was confirmed by 1 % (w/v) agarose gel electrophoresis and by a Bioanalyzer 2100 (Agilent Technologies) using the RNA 6000 Nano LabChip Kit. RNA samples with RIN [?] 6 were considered suitable for sequencing.

Libraries for RNA sequencing were constructed using the TruSeq Stranded mRNA Sample Prep LT Protocol (Illumina), and were sequenced with 2x100 bp paired-end reads on an Illumina HiSeq2500 platform, using a HiSeq Flow Cell v4 with HiSeq SBS Kit v4 (Illumina) at the Centro de Genomica Funcional Aplicada a Agropecuaria e Agroenergia, ESALQ, USP, Brazil.

## Sequence Analysis

Adaptors and low-quality sequences below 23 and 30 Phred quality parameters for maximum average error and maximum error at the end, respectively, were trimmed using SeqClean v.1.9.10 (Zhbannikov *et al.* , 2017). Only high-quality paired-end sequences were used for further analysis. Contaminant sequences were removed using HISAT2 v2.0.5 (Kim *et al.* , 2015). For contaminant identification, a contaminant bank was built containing sequences of Bacteria, Nematoda, Oomycetes, and Platyhelminthes with the assembled complete genome, chromosome, or scaffold from reference or representative genomes (RefSeq category). Data were downloaded in December 2017 using NCBI Entrez Direct E-utilities v6.60 (Kans, 2018). Quality-filtered reads were aligned against the contaminant bank database using the HISAT2 flag "un-conc" to recover paired-end sequences that failed to align concordantly with contaminants. *De novo* transcriptome assembling was generated using Trinity v.2.8.3 (Haas *et al.* , 2013) with default parameters. The longest isoforms were extracted using the TRINITY package script `get_longest_isoform_seq_per_trinity_gene.pl`.

The completeness of our transcriptome assembly was assessed using the Benchmarking Universal Single-Copy Ortholog v5.2.2 (BUSCO, <http://busco.ezlab.org>, Manniet *et al.* , 2021). The *de novo* assembled transcriptome was annotated against the Viridiplantae SwissProt database ([www.uniprot.org](http://www.uniprot.org)) (downloaded on September 18, 2019) using the BLASTX program, of BLAST suite (Camacho *et al.* , 2008), with  $1e^{-5}$  e-value threshold. Annotated assemblies had their GeneOntology (GO) terms retrieved with the tool "Retrieve/ID mapping" on the UniProt website ([www.uniprot.org](http://www.uniprot.org)), and parental terms were recovered using Blast2GO (version 5.2.5) "Combined Graph" tool (Conesa *et al.* , 2005).

Further, functional annotation of *B. magnifica* cambium and differentiating xylem transcriptome was compared to that of the model species *Populus* (*P. x euramericana* ) and *Eucalyptus grandis* annotated by Zinkgraf *et al.* (2017) over the data generated by Xu *et al.* (2014). *A. thaliana* orthologs of each expressed gene from the two model species retrieved by the authors were used to recover the associated GO terms using the UniProt website. For transcriptome comparison, we selected the Biological Process GOs associated with at least 10 % of the transcripts using the Blast2GO "Combined Graph" tool for all three species. A heat map created to visualize the functional comparison between *B. magnifica* , *Populus*, and *Eucalyptus* was produced using the online tool Morpheus (Broad Institute, URL: <https://software.broadinstitute.org/morpheus/>).

For differential expression analysis, the 12 RNA-Seq samples were mapped over the GO term-associated transcripts using Salmon v.0.11.3 (Patro *et al.* , 2017). The transcript abundances were then used to identify the differentially expressed genes (DEGs) between self-supporting and lianescent-phases. The significance of differences was assessed with the package edgeR v.3.26.8 (Robinson *et al.* , 2010) from Bioconductor v.3.9 software (Huber *et al.* , 2015). For this purpose, we normalized the 12 libraries with the TMM method (Robinson & Oshlack, 2010) using the `calcNormFactors()` function, while common dispersions were calculated with the `estimateCommonDisp()` function (Robinson & Smyth, 2008). The threshold adopted

for significance assessing was  $p < 0.05$ , false discovery rate (FDR)  $< 0.05$ , and  $\log_2$  fold change  $> 2$ . GO functional enrichment analysis of DEGs was performed by Fisher exact test (FDR  $< 0.05$ ) using Blast2GO (version 5.2.5).

## Results

### Vessel Size, Distribution, and Fiber Relative Area Differentiate Self-Supporting and Lianescent Xylem

To characterize the phenotypic changes in *B. magnifica* wood, we examined the xylem anatomy of mature stems showing the self-supporting and lianescent xylem. The careful analysis of multiple images of each sectional plane showed that the self-supporting xylem consisted of a matrix of septate fibers and rays, with vessels and scanty paratracheal axial parenchyma produced solely by the fascicular cambium, opposite the primary xylem poles (Fig. 3a, left). This restriction on vessel production was sustained throughout the self-supporting phase, conferring a radial arrangement to the vessels opposite the protoxylem poles. The rays in the self-supporting xylem were uniseriate and composed of upright and square cells (Fig. 3b, left).

In contrast, the onset of the lianescent xylem was marked by the simultaneous production of several large vessels throughout the cambium width by both the fascicular and interfascicular cambium (Fig. 3a, white arrows). These large vessels had a diameter of  $111\mu\text{m}$  and were solitary or associated with small vessels and formed a bimodal distribution of vessel diameter classes (Fig. 3c). The lianescent xylem also had septate fibers, but the rays were uni to biseriate and composed of predominantly procumbent and square cells (Fig. 3b, right).

Quantitative analysis revealed significant differences between the two phases (Table 1). Vessel relative area increased from 5.7% in the self-supporting phase to 35.9% in the lianescent xylem. This increase was mainly at the expense of fiber relative area, which decreased from 81.6% in self-supporting xylem to 54.7% in lianescent xylem. The increase in vessel relative area was primarily driven by vessel size, while vessel density remained constant. Consequently, the potential specific conductivity of the xylem increased more than 20-fold, from  $4.52 \times 10^{-6} \text{ kg m}^{-1}\text{Mpa}^{-1} \text{ s}^{-1}$  in self-supporting xylem to  $106.98 \times 10^{-6} \text{ kg m}^{-1}\text{Mpa}^{-1} \text{ s}^{-1}$  in lianescent xylem. Intervessel-pit diameter and vessel grouping index, both related to water conduction, also increased, while fibers in the lianescent xylem were shorter, wider, and had thicker cell walls compared to the self-supporting xylem. These changes in cell dimensions resulted in an overall reduction in cell density (number of cells per area).

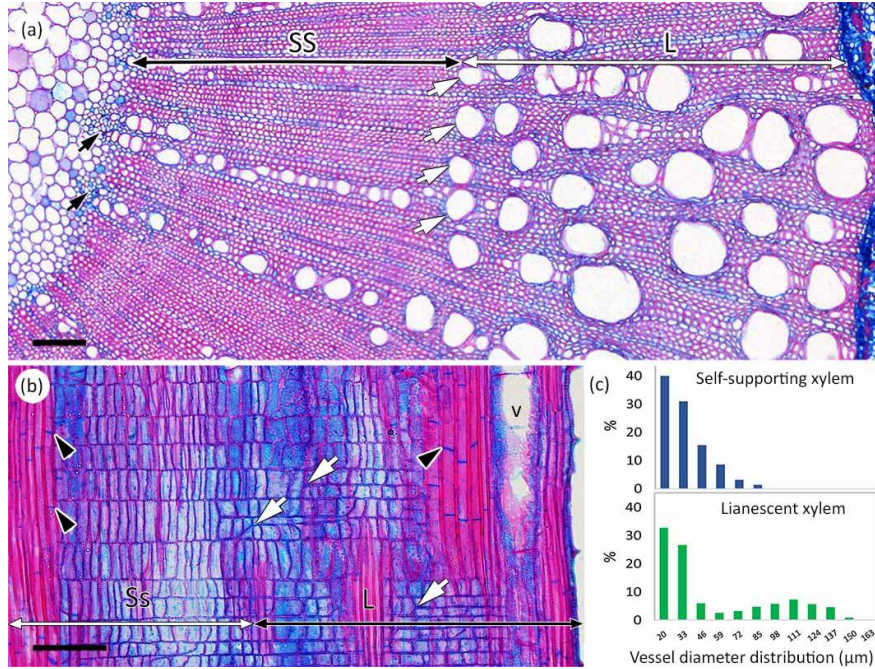


**Fig. 3.** Self-supporting and lianescent xylem anatomy. (a) Stem cross-section showing self-supporting xylem (SS), characterized by small radially arranged vessels formed only by the fascicular cambium, opposite to protoxylem poles (black arrows), and a high proportion of fibers. The beginning of the lianescent xylem (L) is marked by the concomitant production of several large vessels (white arrows) not restricted to radial files and the reduction of fiber amount. The large vessels are associated with small vessels and comprise a larger proportion of the xylem in this phase. (b) Longitudinal radial section of the xylem. Ray composition changes from upright cells in SS to mainly square and procumbent cells in L (white arrows). Septate fibers (arrowheads) are found in both phases. Vessel (v). (c) Self-supporting and lianescent xylem vessel diameter classes distribution. Scale bars: (a) 125  $\mu\text{m}$ ; (b) 100  $\mu\text{m}$ .

This analysis highlights the distinct characteristics of self-supporting and lianescent xylem, including the broader distribution of vessels in the later phase, no longer restricted to the fascicular regions. The production of large vessels in the lianescent phase significantly increased water potential specific conductivity and reduced the number of cells per area.

**Table 1.** Quantitative characterization of self-supporting and lianescent xylem.

Relative areas of different cell types (%)	Self-supporting	Self-supporting	Self-supporting	Self-supporting	Lianescent	Lianescent	Lianescent	Difference between phases (%)
Vessels	5.7 ( $\pm 2.7$ )	5.7 ( $\pm 2.7$ )	35.9 ( $\pm 8.5$ )	35.9 ( $\pm 8.5$ )	35.9 ( $\pm 8.5$ )	529.82 **	529.82 **	529.82
Fibers	81.6 ( $\pm 3.8$ )	81.6 ( $\pm 3.8$ )	54.7 ( $\pm 8.5$ )	54.7 ( $\pm 8.5$ )	54.7 ( $\pm 8.5$ )	-32.97 **	-32.97 **	-32.97

Axial parenchyma	Axial parenchyma	<b>0.6 (±0.4)</b>	<b>0.6 (±0.4)</b>	<b>1.7 (±0.9)</b>	<b>1.7 (±0.9)</b>	<b>183.33 *</b>	<b>183.33 *</b>	<b>183.33 *</b>	
Radial parenchyma		<b>12.0 (±2.5)</b>	<b>7.7 (±1.6)</b>	<b>7.7 (±1.6)</b>	<b>7.7 (±1.6)</b>	<b>-35.83 *</b>	<b>-35.83 *</b>	<b>-35.83 *</b>	
<b>Vessels</b>									
Mean diameter (D - μm)		<b>26.29 (±16.59)</b>	<b>26.29 (±16.59)</b>	<b>45.57 (±37.96)</b>	<b>45.57 (±37.96)</b>	<b>45.57 (±37.96)</b>	<b>73.34 ***</b>	<b>73.34 ***</b>	<b>73.34 ***</b>
Max diameter (D <sub>max</sub> - μm)		<b>73.48 (±12.25)</b>	<b>73.48 (±12.25)</b>	<b>141.20 (±10.96)</b>	<b>141.20 (±10.96)</b>	<b>141.20 (±10.96)</b>	<b>92.16 ***</b>	<b>92.16 ***</b>	<b>92.16 ***</b>
Minimum diameter (D <sub>min</sub> - μm)	7.46 (±1.64)	7.46 (±1.64)	7.63 (±1.18)	7.63 (±1.18)	7.63 (±1.18)	-	-	-	
Hydraulic diameter (D <sub>h</sub> - μm)		<b>38.20 (±6.17)</b>	<b>38.20 (±6.17)</b>	<b>77.70 (±8.23)</b>	<b>77.70 (±8.23)</b>	<b>77.70 (±8.23)</b>	<b>103.40 *</b>	<b>103.40 *</b>	<b>103.40 *</b>
Vessel density (V <sub>d</sub> - v mm <sup>-2</sup> )	81.90 (±30.39)	81.90 (±30.39)	122 (±35.74)	122 (±35.74)	122 (±35.74)	-	-	-	
Vessel grouping index (V <sub>g</sub> )		<b>2.42 (±0.58)</b>	<b>2.42 (±0.58)</b>	<b>3.63 (±0.53)</b>	<b>3.63 (±0.53)</b>	<b>3.63 (±0.53)</b>	<b>50.00 **</b>	<b>50.00 **</b>	<b>50.00 **</b>
Vessel element high (μm)	335.3 (±102.27)	335.3 (±102.27)	327.5 (±72.50)	327.5 (±72.50)	327.5 (±72.50)	-	-	-	
Pit diameter (μm)		<b>4.28 (±0.72)</b>	<b>4.28 (±0.72)</b>	<b>4.95 (±0.79)</b>	<b>4.95 (±0.79)</b>	<b>4.95 (±0.79)</b>	<b>15.65 ***</b>	<b>15.65 ***</b>	<b>15.65 ***</b>
Arrangement	Radial	Radial	-	-	-				
Specific conductivity (K <sub>p</sub> - kg m <sup>-1</sup> Mpa <sup>-1</sup> s <sup>-1</sup> 10 <sup>-6</sup> )	Specific conductivity (K <sub>p</sub> - kg m <sup>-1</sup> Mpa <sup>-1</sup> s <sup>-1</sup> 10 <sup>-6</sup> )	<b>4.52 (±2.70)</b>	<b>4.52 (±2.70)</b>	<b>106.98 (±31.23)</b>	<b>106.98 (±31.23)</b>	<b>2262,81 **</b>	<b>2262,81 **</b>	<b>2262,81 **</b>	
<b>Fibers</b>									
Length (μm)		<b>721.8 (±175.90)</b>	<b>721.8 (±175.90)</b>	<b>661.9 (±124.6)</b>	<b>661.9 (±124.6)</b>	<b>661.9 (±124.6)</b>	<b>-8.30 ***</b>	<b>-8.30 ***</b>	<b>-8.30 ***</b>
Wall thickness (μm)		<b>1.87 (±0.38)</b>	<b>1.87 (±0.38)</b>	<b>2.41 (±0.56)</b>	<b>2.41 (±0.56)</b>	<b>2.41 (±0.56)</b>	<b>28.88 ***</b>	<b>28.88 ***</b>	<b>28.88 ***</b>
Lumen area (μm)		<b>58.6 (±33.17)</b>	<b>58.6 (±33.17)</b>	<b>74.3 (±38.65)</b>	<b>74.3 (±38.65)</b>	<b>74.3 (±38.65)</b>	<b>26.79 ***</b>	<b>26.79 ***</b>	<b>26.79 ***</b>
<b>Rays</b>									
Width	Unisseriate	Unisseriate	Uni and biseriate	Uni and biseriate	Uni and biseriate				

Cellular composition	Upright and square	Upright and square	Predominantly procumbent and square			
----------------------	--------------------	--------------------	-------------------------------------	-------------------------------------	-------------------------------------	-------------------------------------

Measurements were taken at 4/5 of the stem length towards the base of the stem; means and standard deviations are presented. Differences (%) were calculated using the formula  $((L - S_s) S_s^{-1}) \times 100$ . Significant differences are marked in bold. \*:  $p < 0.05$ ; \*\*:  $p < 0.01$ ; \*\*\*:  $p < 0.001$ .

### The Presence of Physical Supports Triggers Lianescent Xylem Formation

To investigate whether the attachment to physical supports triggers the formation of lianescent xylem, we analyzed the secondary xylem anatomy of the longest stems of five supported and five unsupported plants at regular intervals (Fig. 4). Supported plants had longer ( $6.6 \pm 1.6$  [SD] m) and thicker stems ( $10.4 \pm 3.6$  mm) compared to unsupported plants ( $2.7 \pm 0.8$  m long and  $9.4 \pm 0.8$  mm thick).

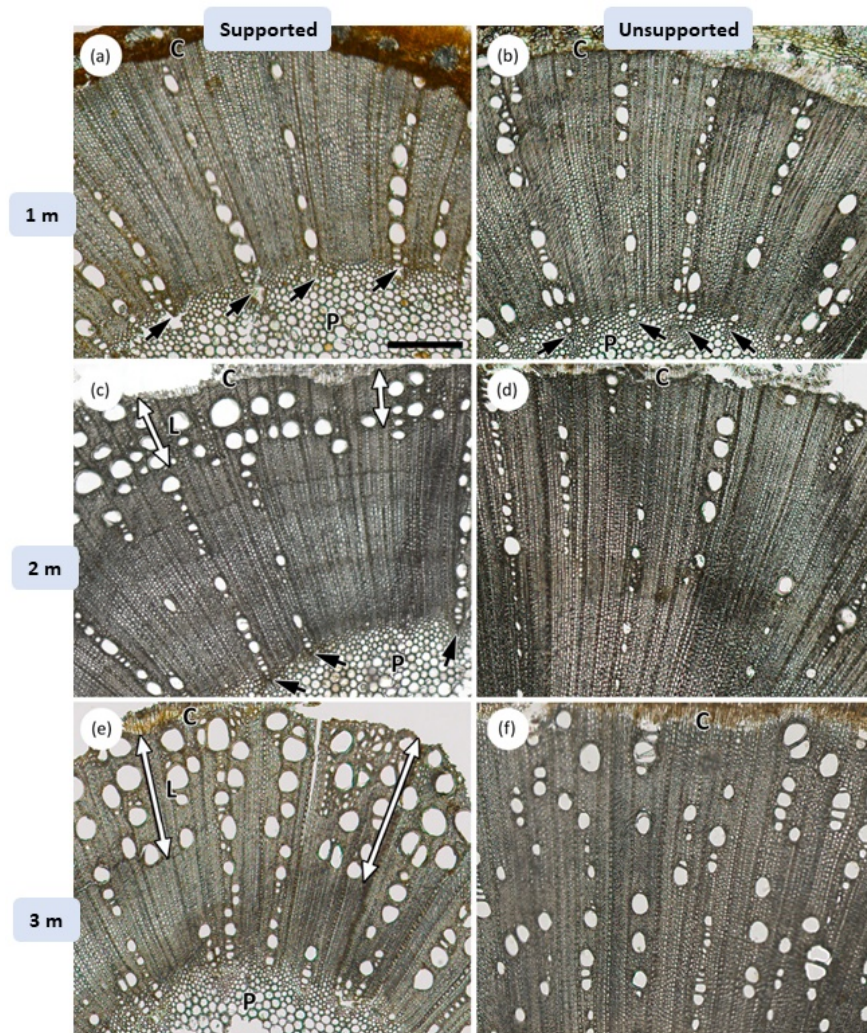


**Fig. 4.** Stem cross sections of supported (a, c, and e) and unsupported plants (b, d, and f) at different

distances from the shoot apex: one meter (a and b), two meters (c and d), and three meters (e and f). Lianescent xylem is produced only in supported plants (white arrows), from 1.5 meters from the apex along the proximal portion of the stem (c and e). In contrast, only self-supporting xylem is produced by unsupported plants (d and f). Note the smaller xylem production in supported plants, measured by the distance between the pith (P, not shown in d and f) and the cambium (C). Scale: 30  $\mu\text{m}$ . Unstained sections.

All plants produced self-supporting xylem near the stem apex (Fig. 5a and b), while the production of lianescent xylem was observed only in plants grown with physical supports. Lianescent xylem formation started from 1.5 – 2 m from the apex and extended through the proximal portion of the stem in supported plants (Fig. 5c and 5e). In contrast, unsupported plants only produced self-supporting xylem along the entire stem (Fig. 5d and 5f).

The production of lianescent xylem was associated with a smaller xylem production, measured as the linear distance between the cambium and the beginning of the secondary xylem (Fig. 5). In contrast, unsupported plants, which only formed the self-supporting xylem, produced more secondary xylem at the same distance from the apex compared to supported plants

These findings indicate that lianescent xylem formation occurs in response to stem attachment to physical supports, leading to reduced cambial activity, increased vessel size, and enhanced xylem conductivity.

### ***B. magnifica* Cambium and Differentiating Xylem Transcriptome is Consistent with Model Tree Species**

To understand the transcriptional regulation underlying the concomitant formation of distinct xylem phases in different parts of the same plant, we conducted an RNA-Seq analysis of the active cambium and differentiating xylem of portions producing the self-supporting or the lianescent xylem. We sequenced six biological samples for each phase, resulting in approximately 512 million paired-end reads (40 GB, Supporting Information Fig. S3, Table S1a). *De novo* assembly produced 133,883 transcripts, from which 54,207 longest isoforms were recovered (Supporting Information Fig. S3). Among these, 20,548 transcripts showed BLASTX hits against Viridiplantae sequences in the SwissProt database (downloaded on September 18, 2019). We identified 20,428 sequences associated with Gene Ontology (GO) terms, which were further analyzed (Supporting Information Fig. S3 and Tables S1a, S1b, S1c). Out of the 7,198 unique GO terms identified, 3,738, 2,714, and 746 were related to biological processes (BP), molecular functions (MF), and cellular components (CC), respectively (Supporting Information Tables S2).

The completeness of the assembled transcriptome was assessed using BUSCO v5.2.2 (Manni *et al.*, 2021), which showed 99% complete BUSCOs (number of BUSCOs: 425), indicating the high quality of our assembly. Among the 20,428 GO-associated sequences, we identified two transcripts homologous to the cambial markers PHLOEM INTERCALATED WITH XYLEM (PXY)/TDIF RECEPTOR (TDR; DN4695.c0.g1.i3 and DN19385.c0.g1.i1; transcript identifiers listed in Supporting Information Table S1b) and one homologous to WUSCHEL RELATED HOMEBOX4 (WOX4; DN4743.c0.g1.i1) (Hirakawa *et al.*, 2010; Suer *et al.*, 2011; Shi *et al.*, 2019; Shi *et al.*, 2021). We also identified the phloem markers ALTERED PHLOEM DEVELOPMENT (APL; DN4491.c0.g1.i2 and DN5859.c0.g1.i6) and NAC domain-containing protein 86 (NAC086; DN12555.c0.g1.i1) (Froelich *et al.*, 2011; Furuta *et al.*, 2014; Shi *et al.*, 2021), indicating successful sampling of cambium and differentiating xylem tissues.

To check the quality of the assembled transcriptome, we compared the functional annotation of *B. magnifica* with those of the secondary xylem-forming tissues from model species *Eucalyptus grandis* and *Populus × euramericana*, following the approach of Zinkgraf *et al.* (2017) using the data generated by Xu *et al.* (2014). The cambium and differentiating xylem transcriptome of *B. magnifica* (20,428 transcripts) exhibited a higher number of transcripts with associated GO terms compared to the other two species (15,127 and 14,186 for *E. grandis* and *P. × euramericana*, respectively). Interestingly, all the most significant BP present in the model species were also found in *B. magnifica*, with a similar number of associated transcripts, whether considering the total transcriptome (*i.e.*, from both phases combined, Fig. 5a) or each phase separately. Additionally, we identified 105 BP exclusively present in *B. magnifica* (Supporting Information Fig. S4),

potentially encompassing transcripts with unique functions in *B. magnifica*.

## The Transcriptome of Self-Supporting and Lianescent Phases of Xylem Development Differs in Their Most Relevant Gene Functions

To identify differentially expressed genes (DEGs) between the self-supporting and lianescent phases, we assessed the diversity of expression profiles within each phase. A multidimensional scaling (MDS) analysis showed a clear grouping of samples within each set, indicating their suitability for further analysis (Supporting Information Fig. S5).

Applying a significance cut-off of  $p < 0.05$ , false discovery rate (FDR)  $< 0.05$ , and  $\log_2 \text{FC} > |2|$  (Fig. 5b), we identified 140 upregulated transcripts in the self-supporting phase and 85 upregulated transcripts in the lianescent phases (Supporting Information Tables S3a, c, respectively; count of annotated transcripts shown in Supporting Information Table S1c). Enrichment analysis revealed that in the self-supporting phase, the most represented GO categories (BP, MF, and CC) could be grouped into cell wall-related processes (overrepresented), transcriptional regulation, and protein metabolism (both underrepresented) (Supporting Information Table S3b). In the lianescent phase, the BP category *response to stimulus*, which includes *response to organic substance*, *response to hormone*, and *response to endogenous stimulus*, was highly overrepresented, suggesting the involvement of hormone signaling in xylem differentiation. The MF *L-glutamine transmembrane transporter activity* was also overrepresented (Supporting Information Table S3d).

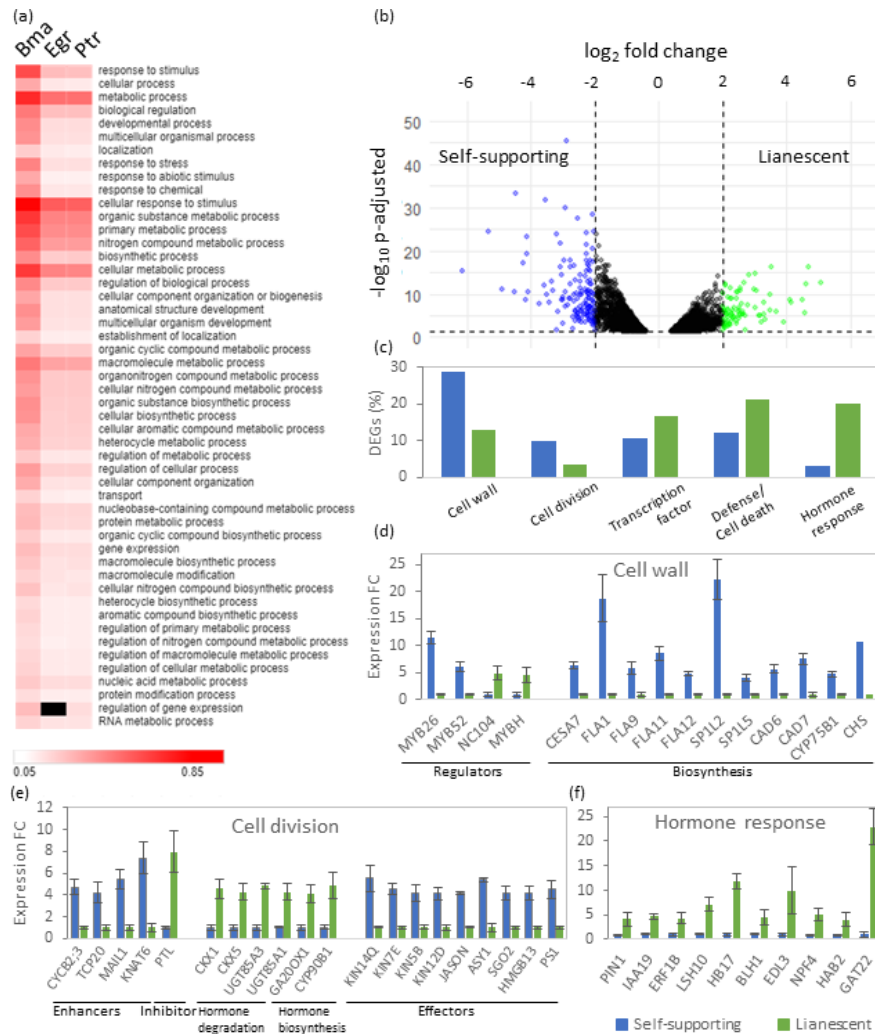


**Fig. 5.** (a) Comparative functional annotation of cambial transcriptomes from *B. magnifica* (Bma) and the model species *Eucalyptus grandis* (Egr) and *Populus × euramericana* (Pop) (using data generated by Xu *et al.* 2014). (b) Volcano plot showing transcript expression p-value versus log2 of fold-change of 240,428 annotated transcripts associated with GO terms. A total of 225 differentially expressed genes (DEGs) were recovered using a cutoff of  $p < 0.05$  and  $\log_2$  fold change  $> |2|$ : 140 up-regulated in self-supporting xylem forming tissue (blue dots) and 85 up-regulated in lianescent xylem forming tissue (green dots). (c) The five most represented categories of manually curated annotation of the 225 DEGs. In total, 154 (68%) DEGs were annotated in these five categories. Histograms in (d), (e), and (f) show the expression fold changes of genes related to cell wall, cell division, and hormone response, respectively. **MYB26/52** : MYB DOMAIN PROTEIN 26/52; **NC104** : NAC DOMAIN-CONTAINING PROTEIN 104/ XYLEM NAC DOMAIN 1; **MYBH** : MYB HYPOCOTYL ELONGATION-RELATED; **CESA7** : CELLULOSE SYNTHASE CATALYTIC SUBUNIT 7; **FLA1/9/11/12** : FASCICLIN-LIKE ARABINOGALACTAN 1/9/11/12; **SP1L2/5** : SPIRAL1-like 2/5; **CAD6/7** : CINNAMYL ALCOHOL DEHYDROGENASE 6/7; **CYP75B1** : FLAVONOID 3'-MONOOXYGENASE; **CHS** : CHALCONE SYNTHASE; **CYCB2;3** : CYCLIN B2;3; **TCP20** : TEOSINTE BRANCHED1/CYCLOIDEA/PROLIFERATING CELL FACTOR1-20; **MAIL1** : MAINTENANCE OF MERISTEMS-LIKE1; **KNAT6** : HOMEODOMAIN PROTEIN KNOTTED-1-LIKE6; **PTL** : PETAL LOSS; **CKX1/5** : CYTOKININ OXIDASE/DEHYDROGENASE 1/5; **UGT85A1/85A3** : UDP-GLUCOSYL TRANSFERASE 85<sup>a</sup>1/85<sup>a</sup>3; **GAOX1** : GA20 OXIDASE 1; **CYP90B1** : CYTOCHROME P450 90B1; **KIN14Q/7E/5B/12D** : KINESIN-LIKE-14Q/7E/5B/12D; **JASON** ; **ASY1** : ASYNAPTIC 1; **SGO2** : SHUGOSHIN 2; **HMGB13** : 3XHIGH MOBILITY GROUP-BOX1; **OS1** : PARALLEL SPINDLE 1; **PIN1** : PIN-FORMED 1; **IAA19** ; **ERF1B** : ETHYLENE-RESPONSIVE TRANSCRIPTION FACTOR 1B; **LSH10** : LIGHT-DEPENDENT SHORT HYPOCOTYLS 10; **HB17** : HOMEODOMAIN-LEUCINE ZIPPER PROTEIN 17; **BLH1** : BEL1-LIKE HOMEODOMAIN; **EDL3** : EID1-LIKE F-BOX PROTEIN 3; **NPF4** : NRT1/ PTR FAMILY 4; **HAB2** : PROTEIN PHOSPHATASE 2C; **GAT22** : GATA TRANSCRIPTION FACTOR 22.

### Upregulation of Cell Division and Cell Wall-Related Transcripts Characterizes the Self-Supporting Phase Transcriptome

To better understand the gene functions that determined the differences between self-supporting and lianescent xylem differentiation, we performed a manually-curated comprehensive annotation of all DEGs against the literature (Supporting Information Table S3a, c, column J). In line with the higher number of cells per area and the consequent greater cell wall deposition in self-supporting xylem, 11 % and 30 % of the DEGs are associated with cell division and cell wall, contrasting with only 4 % and 18 % in the lianescent counterpart, respectively (Fig. 5c, Supporting Information Table S4).

Among the DEGs associated with cell division in the self-supporting phase, we found two transcripts homologous to positive regulators of the cell cycle, the mitotic-specific cyclin *CYCB2;3* and the transcription factor (TF) *TEOSINTE BRANCHED1/CYCLOIDEA/PROLIFERATING CELL FACTOR1-20* (*TCP20*) (DN860.c0.g2.i2 and DN10604.c0.g1.i2, respectively; Fig. 5e). We also found two transcripts whose homologs are related to meristem identity and activity maintenance, a homolog of the nuclear protein *MAINTENANCE OF MERISTEMS-LIKE1* (*MAIL1*, DN8697.c0.g1.i3), and a homolog to the TF *HOMEODOMAIN PROTEIN KNOTTED-1-LIKE6* (*KNAT6*, DN15272.c0.g1.i2), besides four mitotic specific kinesin homologs (*KIN14Q*, *KIN7E*, *KIN5B*, *KIN12D*; DN13653.c1.g1.i1, DN12012.c0.g1.i1, DN11506.c0.g1.i1, and DN13654.c0.g1.i2, respectively) and five chromatin segregation related proteins (*JASON*, *ASY1*, *SGO2*, *HMGB13*, *PS1*; DN1459.c0.g2.i1, DN5155.c0.g1.i1, DN19359.c0.g1.i1, DN5075.c0.g1.i1, and DN2177.c0.g1.i1, respectively; Fig. 5e).

Two transcripts homologs to *MYB* TFs involved in the regulation of SCW biosynthesis, *MYB26*, and *MYB52*, were upregulated in the self-supporting phase (DN7293.c0.g2.i4 and DN35518.c0.g1.i1 respectively; Fig. 5d). Forty upregulated transcripts are directly involved in the SCW biosynthesis and structural modification, among which we highlight homologs of cellulose synthase A (*CESA7*, DN8977.c0.g2.i4), four fasciclin-like arabinogalactan homolog proteins (*FLA1*, *FLA9*, *FLA11*, *FLA12*; DN7969.c0.g1.i2, DN10033.-

c0\_g1.i1, DN49576\_c0\_g1.i1, and DN52901\_c0\_g1.i1, respectively), and two SPIRAL1-like (SP1L2 and SP1L5, DN1885\_c0\_g1.i2 and DN7226\_c0\_g1.i1 respectively; Fig. 5d).

### Upregulation of Response to Stimulus, Hormone-Responsive, and Defense/Cell Death-Related Transcripts Characterizes Lianescent Phase Transcriptome

Manually-curated annotation of the lianescent phase transcriptome showed a higher proportion of TF and hormone-responsive genes, respectively, 17 % and 30 % of all DEGs of this phase, in contrast to only 11 % and 4 % in the self-supporting counterpart. Additionally, 25 % of the DEGs identified in the lianescent phase correspond to genes involved in defense/cell death mechanisms, compared to only 18 % of the DEGs in this category in the self-supporting phase (Fig. 5c, Supporting Information Table S4).

Our analysis revealed important cell differentiation regulators homologs among the upregulated DEGs that may be responsible for the fewer cell divisions and the production of larger vessels in the lianescent xylem. The repressor of cambial cell proliferation PETAL LOSS (PTL; Fig. 5e) and NAC DOMAIN-CONTAINING PROTEIN 104/ XYLEM NAC DOMAIN 1 (NC104; Fig. 5d), which delay SCW production and programmed cell death (PCD), had homologs upregulated in this phase (DN52789\_c0\_g1.i1 and DN10071\_c0\_g1.i1, respectively). *ACAULIS5* (*ACL5*) was another gene responsible for preventing premature PCD with an upregulated homolog in the lianescent phase, although with a logFC of 1.1. Another candidate TF that may be related to large vessel formation was DN31217\_c0\_g1.i1, a homolog of the *A. thaliana* MYB HYPOCOTYL ELONGATION-RELATED (MYBH; Fig. 5d), that induces cellular growth triggered by auxin accumulation.

Fourteen upregulated transcripts have been annotated as TF homologs, six described as hormone-responsive: IAA19 (DN53387\_c0\_g1.i1), GATA TRANSCRIPTION FACTOR 22 (GAT22, DN16098\_c0\_g1.i1), ETHYLENE-RESPONSIVE TRANSCRIPTION FACTOR 1B (ERF1B, DN35952\_c0\_g1.i1), LIGHT-DEPENDENT SHORT HYPOCOTYLS 10 (LSH10, DN507\_c0\_g1.i1), HOMEODOMAIN-LEUCINE ZIPPER PROTEIN 17 (HB17, DN11122\_c0\_g1.i1), and BEL1-LIKE HOMEODOMAIN (BLH1, DN13026\_c0\_g1.i2). These TFs are responsive to indole-3-acetic acid (IAA), cytokinin (CK), ethylene (ET), brassinosteroid (BR), and abscisic acid (ABA, HB17 and BLH1), respectively (Fig. 5f).

Not only hormone-responsive TF homologs were upregulated, but also homologs to transcripts related to hormone metabolism and signaling pathways. CK was the hormone with the highest number of annotated transcripts related to its catabolism/deactivation: two cytokinin dehydrogenases and two UDP-glycosyltransferases homologs (CKX1, CKX5, UGT85A1, UGT85A3; DN20233\_c0\_g1.i1, DN9178\_c0\_g1.i1, DN17065\_c0\_g1.i1, DN49211\_c0\_g1.i1 respectively). Upregulation of homologs to BR and gibberellin (GA) biosynthetic genes were also identified, CYTOCHROME P450 90B1 and GA20 OXIDASE 1 (GAOX1) respectively (DN4579\_c0\_g1.i1, DN11261\_c0\_g1.i1; Fig. 5e), as well as three genes that participate in the ABA signaling pathway, EID1-LIKE F-BOX PROTEIN 3 (*EDL3*), ABA-IMPORTING TRANSPORTER 1 (*AIT1*) and HOMOLOGY TO ABI2 (*HAB2*) (DN45297\_c0\_g1.i1, DN10749\_c0\_g1.i1, and DN10194\_c0\_g1.i5, respectively). Another highlight was the upregulation of the auxin efflux carrier PIN1 homolog (DN10775\_c0\_g1.i1; Fig. 5f), showing the relevance of all major plant hormones in the lianescent xylem differentiation process.

Together, these results show the prevalence of cell division and SCW biosynthesis during the formation of self-supporting xylem and the more complex regulation of the lianescent xylem formation, with the predominance of TF and hormone-responsive genes in this phase.

### Discussion

In the present work, we characterize how the attachment to physical support leads to the production of the lianescent xylem in the liana species *Bignonia magnifica*. We have also demonstrated that the more complex anatomy of the lianescent xylem results from a more complex transcriptional regulation involving the upregulation of transcriptional factors and hormone-responsive genes.

Our finding that the attachment to physical supports signals the onset of lianescent xylem production in *B.*

*magnifica* (Bignoniaceae), a species that employs leaflets modified into tendrils to climb, is similar to that recently observed in the also tendrilate liana *Serjania Mexicana* (Sapindaceae; Rajput *et al.* 2021) and in the stem twinner *Condylocarpon guianense* (Apocynaceae; Soffiatti *et al.*, 2022). This mechanical and functional convergence in lianas from different families and with different climbing strategies highlights the relevance of the environmental perception in the habit. The attachment to external supports relaxes the initial mechanical function of the xylem, representing an important resource economy in the construction of supportive tissue for lianas and allowing the specialization in hydraulic conduction. The phenotypic plasticity represented by the retention of the mechanical function in young searcher stems and the control of lianescent xylem formation only by stems attached to external supports, in turn, allows to better explore the environment and can be viewed as an important ecological and evolutionary strategy, considering the high prevalence of this character among lianas (Caballé, 1993, 1998).

The *ca.* 30% reduction of fibers relative area represented the replacement of this cell type by large vessels, stressing the hydraulic conduction specialization (Ewers *et al.* , 1989, 1990; Ewers and Fisher 1991; Gasson and Dobbins, 1991; Fisher and Ewers, 1995, Lens *et al.* ,2011) over the mechanical function. Pit diameter increase might enhance hydraulic conductivity as well, as pit conductivity resistance accounts for about 80% of the total resistance (Choat *et al.*, 2006), while it might also increase the probability of embolism spread (Wheeler *et al.* 2005; Choat *et al.* 2005; Hacke *et al.* 2006). Similarly, the connectivity of the vessel network, as indicated by the vessel grouping index, increases pathway redundancy and conductivity safety (Carlquist, 1985; Ewers *et al.* , 2007; Wason *et al.* , 2021). However, this trend is limited, as enhanced redundancy can be counteracted by the facilitated spread of embolism through the interconnected vessels above a certain threshold (Mrad *et al.* 2021). Finally, the increase in fiber wall thickness was in contrast to what was found in other lianas (Gartner, 1991; Ménard *et al.* , 2009), but it may have a role in preventing embolisms, since volume allocation to fiber walls increases embolism resistance (Janssen *et al.* , 2020). Our findings highlight the complex relationship between anatomical characteristics, hydraulic conductivity, and gene expression, providing insights into the differentiation of self-supporting and lianescent xylems.

The self-supporting and lianescent xylems showed distinct expression patterns. We have visually summarized the main findings of our differential expression analysis, establishing correlations between them and the observed anatomical changes during the transition from the self-supporting to lianescent phase in *B. magnifica* xylem (Fig. 6). The self-supporting xylem shows a higher level of cellular division, evidenced by the increased secondary xylem production and a composition comprising fibers and small diameter vessels, resulting in a greater cell density per unit area. This pattern is in accordance with the upregulation of homologs of the mitotic-specific cyclin *CYCB2;3* (Van Leene *et al.* 2010) and of the cell cycle regulator *TCP20* (Guan *et al.* 2017), increasing cambial cell divisions in this phase. In this sense, the upregulation of homologs of mitotic-specific kinesins and chromatin segregation-related proteins were also identified. On the other hand, the lianescent-phase transcriptome showed the upregulation of a homolog of the cambial cell proliferation repressor *PTL* (Zhang *et al.* , 2019), and four different CK catabolism/deactivation homolog transcripts, *CKX1/5* and *UGT85A1/85A3*. CKs have long been known to induce cambial activity (Torrey & Loomis, 1967; Aloni *et al.* , 1990), and reduced concentrations of bioactive CKs result in decreased secondary growth in both *Arabidopsis* and *Populus* (Matsumoto-Kitano *et al.* , 2008; Nieminen *et al.* , 2008).

The higher number of cells in the self-supporting phase is expected to correlate with more abundant cell wall biosynthesis. In this sense, homologs of master MYB TFs, *MYB26* and *MYB52* , involved in the regulation of SCW biosynthesis (Yang *et al.* , 2007, 2017; Cassan-Wang *et al.* , 2013), were found to be upregulated in the self-supporting phase. This upregulation was accompanied by the higher expressions of cellulose synthase A homologs and four fasciclin-like arabinogalactan proteins that have been proposed to contribute to stem strength and stiffness in *Eucalyptus* and *A. thaliana* by increasing cellulose deposition and affecting cell-wall matrix integrity (Macmillan *et al.* , 2010). This expression pattern is compatible with the higher stiffness of young liana stems and with the colonizing role of searcher branches in nature (Caballé, 1993, 1998; Rowe & Speck, 1996, 2005; Soffiatti *et al.* , 2022). Interestingly, two *SPR1* homolog transcripts required for the anisotropic cell growth (Nakajima *et al.* , 2004) were upregulated in the self-supporting phase. *SPR1* overexpression increases cell elongation, in accordance with the longer fibers found in the self-supporting

xylem, while *spr* loss-of-function mutants show helical growth of epidermal cells and entire organs (Smyth, 2016), a characteristic of twining vine stems that has long been known (Darwin, 1875; Isnard & Silk, 2009).

The most striking feature of the lianescent xylem is the production of large vessel elements, which dramatically increased potential specific conductivity and vessel relative area. The transcriptional regulation of cell death is an essential aspect of the overall xylem maturation program, which also encompasses cell expansion and SCW deposition, and emphasizes the crucial role of inhibiting cell death during this process (Bollhöner *et al.*, 2012). Besides the upregulation of NC104/XND1, which represses cell wall production and PCD (Zhang *et al.*, 2020; Zhong *et al.*, 2021), ACAULIS5 (ACL5), another gene responsible for preventing premature PCD (Muñiz *et al.*, 2008), was upregulated in the lianescent phase. The increase in cell expansion period before PCD was linearly correlated with the lumen area in *Picea* trees tracheids (Anfodillo *et al.*, 2013; Buttò *et al.*, 2019). Yet, a homolog of MYBH TF, which was shown to trigger cell growth through IAA accumulation (Kwon *et al.*, 2013, Lu *et al.*, 2014), was also upregulated in the lianescent phase and might also be involved in the differentiation of larger vessels.

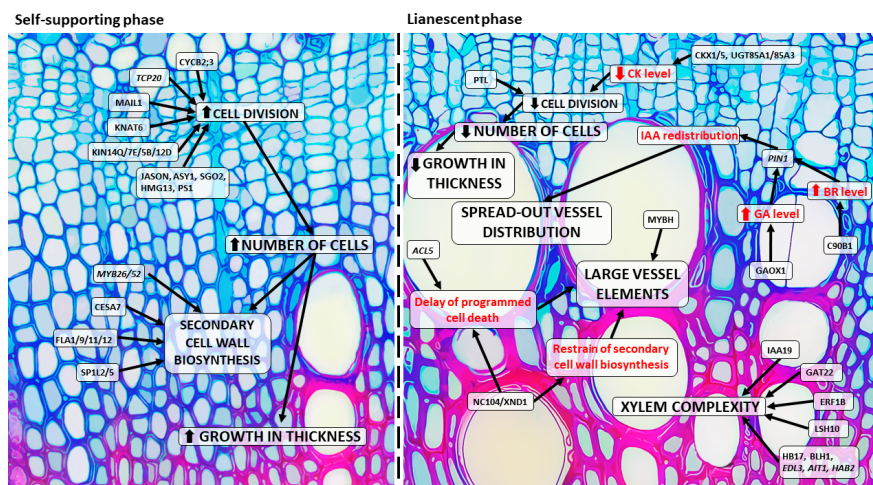


**Fig. 6.** Transcriptional regulatory network model for the self-supporting and lianescent xylem formation in the stems of the liana *B. magnificabased* based on differential gene expression results and comprehensive anatomical analysis. The self-supporting phase has a higher growth in thickness and is composed mainly of fibers and small vessels arranged in radial files in front of protoxylem poles. Self-supporting xylem formation is associated with a higher expression of cell division and secondary cell wall biosynthesis-related transcripts. The lianescent phase has slower growth in thickness and is composed of a smaller fraction of fibers and a higher proportion of vessels. This change is due to the production of large vessels, which are produced throughout the cambium circumference. The formation of lianescent xylem is linked to a much more complex transcription network involving transcription factors, hormone-responsive genes, delayed programmed cell death, and redistribution of auxin-mediated by PIN proteins. Capital letters: observed morphoanatomical characters; in red: deduced characters. **CYCB2;3** : CYCLIN B2;3; **TCP20** : TEOSINTE BRANCHED1/CYCLOIDEA/PROLIFERATING CELL FACTOR1-20; **MAIL1** : MAINTENANCE OF MERISTEMS-LIKE1; **KNAT6** : HOMEBOX PROTEIN KNOTTED-1-LIKE6; **KIN14Q/7E/5B/12D** : KINESIN-LIKE-14Q/7E/5B/12D; **JASON** ; **ASY1** : ASYNAPTIC 1; **SGO2** : SHUGOSHIN 2; **HMGB13** : 3XHIGH MOBILITY GROUP-BOX1; **PS1** : PARALLEL SPINDLE 1; **MYB26/52** : MYB DOMAIN PROTEIN 26/52; **CESA7** : CELLULOSE SYNTHASE CATALYTIC SUBUNIT 7; **FLA1/9/11/12** : FASCICLIN-LIKE ARABINOGALACTAN 1/9/11/12; **SP1L2/5** : SPIRAL1-LIKE2/5; **PTL** : PETAL LOSS; **CKX1/5** : CYTOKININ OXIDASE/DEHYDROGENASE 1/5; **UGT85A1/85A3** : UDP-GLUCOSYL TRANSFERASE 85A1/85A3; **GAOX1** : GA20 OXIDASE 1; **C90B1** : CYTOCHROME P450 90B1; **PIN1** : PIN-FORMED 1; **ACL5** : ACAULIS5; **NC104/XND1** :

NAC DOMAIN-CONTAINING PROTEIN 104/ XYLEM NAC DOMAIN 1; **MYBH** : MYB HYPOCOTYL ELONGATION-RELATED; **HB17** : HOMEODOMAIN-LEUCINE ZIPPER PROTEIN 17; **BLH1** : BEL1-LIKE HOMEODOMAIN; **IAA19** ; **GAT22** : GATA TRANSCRIPTION FACTOR 22; **ERF1B** : ETHYLENE-RESPONSIVE TRANSCRIPTION FACTOR 1B; **LSH10** : LIGHT-DEPENDENT SHORT HYPOCOTYLS 10.

IAA polar flow also seems to be modified in the lianescent phase, as indicated by the upregulation of the polar auxin transporter PINFORMED1 (PIN1). Various processes take place along a PIN1-driven auxin flow, including bundle differentiation (Sachs, 1981; Scarpella *et al.* , 2006), cambium formation and maintenance (Snow, 1935; Uggla *et al.* , 1996; Ko *et al.* , 2004; Mazur *et al.* , 2014; Ye & Zhong, 2015), and the differentiation of vessels bypassing wounds (Mazuret *et al.* , 2016). Hence, vascular differentiation can be used as a marker of auxin flow (Sachs, 2000). Similarly, vessels in the secondary xylem are formed by the coordinated differentiation of thousands of cells, *i.e.* the vessel elements, in a continuous longitudinal series that can reach several meters in lianas (Zimmermann & Jeje, 1981; Ewers *et al.* , 1990). PIN1 upregulation is likely related to the higher number of xylem mother cell derivatives differentiating into vessel elements, leading to the broader distribution of vessels observed in the lianescent xylem. This result reinforces those previously reported suggesting that polar auxin transport defines vessel distribution and size in the secondary xylem (Johnson *et al.* , 2018; Novitskaya *et al.* , 2020).

Transcription factors are central nodes in the transcriptional network responsible for cell identity and differentiation in the xylem (Xie *et al.* , 2021). Here we found 14 TF upregulated in the lianescent phase, six of which participate in hormone-response pathways: two homologs to ABA response regulators, *HB17* and *BLH1* , which also responds to CK (Hoth *et al.* , 2003; Park *et al.* , 2013); a CYTOKININ-RESPONSIVE GATA FACTOR 1 (*GAT22* ) homolog, which was shown to have a regulatory role downstream from both IAA and GA signaling pathways (Richter *et al.* , 2013); a homolog to ethylene-responsive transcription factor ERF1B, which was found to increase IAA production (Mao *et al.* . 2016) and integrates ET and JA pathways (Lorenzo *et al.* 2003); a homolog to the IAA repressor IAA19; and a homolog to the BR responsive TF *LSH10* , which was recently found to be a co-repressor of target genes by its epigenetic regulation (Goda *et al.* , 2004; Vo Phan *et al.* , 2023).

The crosstalk between TFs and various plant hormones in lianescent xylem differentiation was further supported by the upregulation of gene homologs associated with hormone biosynthesis and signaling pathway. Homologs to GAOX1 and C90B1, responsible for GA and BR biosynthesis, respectively, were upregulated in this phase. GA is known to act synergistically with IAA, increasing *PIN1* expression and polar auxin transport (Willige *et al.* , 2011; Mäkilä *et al.* , 2023), conserving cambium homeostasis and xylem differentiation (Ben-Targem *et al.* , 2021), and induces the expression of the same genes as auxin feeding experiments in *Populus* (Bjorklund *et al.* , 2007). Similarly, BR regulates PIN protein expression and high levels of IAA signaling in the cambium (Li *et al.* , 2005; Lee *et al.* , 2021), cellular differentiation and SCW biosynthesis (Yamamoto *et al.* , 1997; Caño-Delgado *et al.* , 2004; Du *et al.* , 2020), and affects CK biosynthesis and catabolism genes (Wang *et al.* , 2022). ABA, which is known as a crucial hormone to drought stress response, was recently shown to regulate the SCW formation under drought conditions (Yu *et al.* , 2021; Liu *et al.* , 2021), besides modulating the expression of target genes that affect vessel traits by inducing the expression of the AREB1 TF (Li *et al.* , 2019). Two ABA signaling pathway regulators, HAB2 and EDL3 (Saez *et al.* , 2004; Yoshida *et al.* , 2006; Koops *et al.* , 2011) were upregulated in the lianescent phase, what may indicate the cooption of the drought response pathway for the higher range of vessel diameters produced in the lianescent phase.

## Concluding Remarks

In the present study, we verified the profound impacts of physical support on the liana *B. magnifica* wood anatomy, promoting the formation of the lianescent xylem. The detailed characterization of xylem anatomy showed that the onset of the lianescent phase is characterized by the beginning of vessel production also by the interfascicular cambium, previously restricted to the fascicular cambium; by the formation of large vessels of a new diameter class, that drastically increases potential specific conductivity; and by a lesser amount

of cambial divisions. The comprehensive integration of anatomical and differential expression analysis data allowed us to propose a model to characterize the molecular control of the lianescent vascular syndrome establishment (Fig. 6). Our model shows that the more complex lianescent xylem reflects a more intricate transcriptional regulation network, involving a more diverse repertoire of TFs and hormone-responsive genes. We hope the analysis of the transcriptional control of the vascular system differentiation in lianas helps to better understand the differentiation of the vascular system in other habits, in addition to shedding light on the formation of the structural diversity present in tropical forests, widely recognized as a center of global diversity.

### Acknowledgments

We thank Dr. Paula Elbl for critical inputs to this study and Dr. Horácio Montenegro for his contribution to computational infrastructure. This study was supported by the São Paulo Research Foundation — FAPESP (Process 18/06917-7), by the Coordenação de Aperfeiçoamento de Pessoal de Nível Superior – Brasil (CAPES) – Finance Code 001, and by The National Council for Scientific and Technological Development — CNPq (process 142223/2015-8).

### Author contribution

ACL and VA conceived the project. ACL and MR designed the experiments. ACL, CSG, and VA analyzed and interpreted anatomical data. Sequence analyses were carried out by ACL, DTS, and SCSA. LLC granted access to the computational facility and was responsible for data curation. ACL and MR interpreted differential gene expression analysis (DEG) results and conducted the hand-curated annotation of DEGs. ACL wrote the article with inputs from MR, CSG, SCSA, and VA. All authors read and approved the final manuscript.

### Data availability

The raw reads from the 12 samples used in this study are publicly available at the Sequence Read Archive (NCBI-SRA), bioproject accession number PRJNA927333 (submitted on 01/25/2023).

### References

- Allona I, Quinn M, Shoop E, Swope K, Cyr SS, Carlis J, Riedl J, Retzel E, Campbell Mm, Sederoff R, Whetten RW. 1998. Analysis of xylem formation in pine by cDNA sequencing. *Proceedings of the National Academy of Sciences* **95**: 9693-9698.
- Aloni R, Baum SF, Peterson CA. 1990. The role of cytokinin in sieve tube regeneration and callose production in wounded *Coleus* internodes. *Plant Physiology* **93**: 982-989.
- Anfodillo T, Petit G, Crivellaro A. 2013. Axial conduit widening in woody species: a still neglected anatomical pattern. *Iawa Journal* **34**: 352-364.
- Angyalossy V, Pace MR, Lima AC. 2015. Liana anatomy: a broad perspective on structural evolution of the vascular system. In Schnitzer SA, Bongers F, Burnham RJ, Putz FE, eds. *Ecology of Lianas*. Chichester, UK: John Wiley & Sons Ltd, 253-287.
- Baas P, Ewers FW, Davis SD, Wheeler EA. 2004. Evolution of xylem physiology. In Hemsley AR, Poole I, eds. *The Evolution of Plant Physiology*. London, UK: Elsevier Academic Press: 273-395.
- Barbosa ACF, Pace MR, Witovsk L, Angyalossy V. 2010. A new method to obtain good anatomical slides of heterogeneous plant parts. *IAWA Journal* **31**: 373-383.
- Beeckman H. 2016. Wood anatomy and trait-based ecology. *IAWA journal* **37**: 127-151.
- Ben-Targem M, Ripper D, Bayer M, Ragni L. 2021. Auxin and gibberellin signaling cross-talk promotes hypocotyl xylem expansion and cambium homeostasis. *Journal of Experimental Botany* **72**:3647-3660.

**Berlyn GP, Miksche JP. 1976.** Botanical microtechnique and cytochemistry. Ames, USA: Iowa State University Press.

**Björklund S, Antti H, Uddestrand I, Moritz T, Sundberg B. 2007.** Cross-talk between gibberellin and auxin in development of *Populus* wood: gibberellin stimulates polar auxin transport and has a common transcriptome with auxin. *The Plant Journal* **52**: 499-511.

**Bollhoner B, Prestele J, Tuominen H. 2012.** Xylem cell death: emerging understanding of regulation and function. *Journal of Experimental Botany* **63**: 1081-1094.

**Bukatsch F. 1972.** Bemerkungem zur Doppelfärbung Astra-blau-Safranin. *Mikrokosmos* **6**: 255.

**Butto V, Rossi S, Deslauriers A, Morin H. 2019.** Is size an issue of time? Relationship between the duration of xylem development and cell traits. *Annals of Botany* **123**: 1257-1265.

**Caballe G. 1993.** Liana structure, function and selection: a comparative study of xylem cylinders of tropical rainforest species in Africa and America. *Botanical Journal of the Linnean Society* **113**: 41-60.

**Caballe G. 1998.** Le port autoportant des lianes tropicales: une synthèse des stratégies de croissance. *Canadian Journal of Botany* **76**: 1703-1716.

**Camacho C, Madden T, Ma N, Tao T, Agarwala R, Morgulis A. 2008.** BLAST (r) Command Line Applications User Manual. (National Center for Biotechnology Information (US), 2008). URL <https://www.ncbi.nlm.nih.gov/books/NBK279690/>

**Cano-Delgado A, Yin Y, Yu C, Vafeados D, Mora-Garcia S, Cheng, JC, Nam KH, Li J, Chory J. 2004.** BRL1 and BRL3 are novel brassinosteroid receptors that function in vascular differentiation in *Arabidopsis*. *Development* **131**: 5341-5351.

**Carlquist S. 1981.** Wood anatomy of Nepenthaceae. *Bulletin of the Torrey Botanical Club* **108**: 324-330.

**Carlquist S. 1985.** Observations on functional wood histology of vines and lianas: vessel dimorphism, tracheids, vasicentric tracheids, narrow vessels, and parenchyma. *Aliso* **11**: 139-157.

**Carpentier SC, Panis B, Vertommen A, Swennen R, Sergeant K, Renaut J, Laukens K, Witters E, Samyn B, Devreese, B. 2008.** Proteome analysis of non-model plants: a challenging but powerful approach. *Mass spectrometry reviews* **27**: 354-377.

**Cassan-Wang H, Goue N, Saidi MN, Legay S, Sivadon P, Goffner D, Grima-Pettenati J. 2013 .** Identification of novel transcription factors regulating secondary cell wall formation in *Arabidopsis*. *Frontiers in plant science* **4**: 189.

**Choat B, Brodie TW, Cobb AR, Zwieniecki MA, Holbrook NM. 2006.** Direct measurements of intervessel pit membrane hydraulic resistance in two angiosperm tree species. *American journal of botany* **93**: 993-1000.

**Choat B, Lahr EC, Melcher PJ, Zwieniecki MA, Holbrook NM. 2005.** The spatial pattern of air seeding thresholds in mature sugar maple trees. *Plant, Cell & Environment* **28**: 1082-1089.

**Conesa A, Gotz S, Garcia-Gomez JM, Terol J, Talon M, Robles M. 2005.** Blast2GO: a universal tool for annotation, visualization and analysis in functional genomics research. *Bioinformatics* **21**: 3674-3676.

**Darwin C. 1875.** *The movements and habits of climbing plants* . London, UK: J. Murray.

**Du J, Gerttula S, Li Z, Zhao ST, Liu YL, Liu Y, Lu MZ, Groover AT. 2020.** Brassinosteroid regulation of wood formation in poplar. *New Phytologist* **225**: 1516-1530.

**Evert RF. 2006.** *Esau's plant anatomy: meristems, cells, and tissues of the plant body: their structure, function, and development* . New Jersey, USA: John Wiley & Sons.

- Ewers FW, Ewers JM, Jacobsen AL, Lopez-Portillo J. 2007.** Vessel redundancy: modeling safety in numbers. *IAWA Journal* **28**:373-388.
- Ewers FW, Fisher JB. 1991.** Why vines have narrow stems: histological trends in *Bauhinia* (Fabaceae). *Oecologia* **88** :233–237.
- Ewers FW, Fisher JB, Chuis TS. 1989.** Water transport in the liana *Bauhinia fassoglensis* (Fabaceae). *Plant Physiology* **91** :1625–1630.
- Ewers FW, Fisher JB, Chiu ST. 1990.** A survey of vessel dimensions in stems of tropical lianas and other growth forms. *Oecologia* **84**: 544-552.
- Fisher J, Ewers F. 1995.** Vessel dimensions in liana and tree species of *Gnetum*(Gnetales). *American Journal of Botany* **82**: 1350–1357.
- Froelich DR, Mullendore DL, Jensen KH, Ross-Elliott TJ, Anstead JA, Thompson GA, Pelissier HC, Knoblauch M. 2011.** Phloem ultrastructure and pressure flow: Sieve-Element-Occlusion-Related agglomerations do not affect translocation. *Plant Cell* **23**: 4428-4445.
- Furuta KM, Yadav SR, Lehesranta S, Belevich I, Miyashima S, Heo JO, Vaten A, Lindgren O, De Rybel B, Van Isterdael G et al. 2014.** Plant development. Arabidopsis NAC45/86 direct sieve element morphogenesis culminating in enucleation. *Science* **345**:933–937.
- Gartner BL. 1991.** Structural stability and architecture of vines vs. shrubs of poison oak, *Toxicodendron diversilobum*. *Ecology* **72**: 2005-2015.
- Gasson P, Dobbins DR. 1991.** Wood anatomy of the Bignoniaceae, with a comparison of trees and lianas. *IAWA Bulletin* **12**:389–417.
- Gentry AH. 1986.** Species richness and floristic composition of Choco region plant communities. *Caldasia* **15**: 71-91.
- Gerolamo CS, Angyalossy V. 2017.** Wood anatomy and conductivity in lianas, shrubs and trees of Bignoniaceae. *IAWA Journal* **38**: 412-432.
- Goda H, Sawa S, Asami T, Fujioka S, Shimada Y, Yoshida S. 2004.** Comprehensive comparison of auxin-regulated and brassinosteroid-regulated genes in Arabidopsis. *Plant physiology* **134**: 1555-1573.
- Groover AT. 2005.** What genes make a tree a tree? *Trends in plant science* **10**: 210-214.
- Guan P, Ripoll JJ, Wang R, Vuong L, Bailey-Steinitz LJ, Ye D, Crawford NM. 2017.** Interacting TCP and NLP transcription factors control plant responses to nitrate availability. *Proceedings of the National Academy of Sciences* **114**: 2419-2424.
- Haas BJ, Papanicolaou A, Yassour M, Grabherr M, Blood PD, Bowden J, Couger MB, Eccles D, Li B, Lieber M et al. 2013.** De novo transcript sequence reconstruction from RNA-seq using the Trinity platform for reference generation and analysis. *Nature protocols* **8**: 1494.
- Hacke UG, Sperry JS, Wheeler JK, Castro L. 2006.** Scaling of angiosperm xylem structure with safety and efficiency. *Tree physiology* **26**: 689-701.
- Hirakawa Y, Bowman JL. 2015.** A role of TDIF peptide signaling in vascular cell differentiation is conserved among euphyllphytes. *Frontiers in plant science* **6**: 1048.
- Hirakawa Y, Kondo Y, Fukuda H. 2010.** TDIF peptide signaling regulates vascular stem cell proliferation via the WOX4 homeobox gene in Arabidopsis. *The Plant Cell* **22**: 2618-2629.
- Hoth S, Ikeda Y, Morgante M, Wang X, Zuo J, Hanafey MK, Gaasterland T, Tingey SV, Chua NH. 2003.** Monitoring genome-wide changes in gene expression in response to endogenous cytokinin reveals targets in Arabidopsis thaliana. *FEBS Letters* **554**: 373-380.

- Hu R, Qi G, Kong Y, Kong D, Gao Q, Zhou G. 2010.** Comprehensive analysis of NAC domain transcription factor gene family in *Populus trichocarpa*. *BMC plant biology* **10**: 145.
- Huber W, Carey VJ, Gentleman R, Anders S, Carlson M, Carvalho BS, Bravo HC, Davis S, Gatto L, Girke T et al. 2015.** Orchestrating high-throughput genomic analysis with Bioconductor. *Nature methods* **12**: 115.
- IAWA Committee. 1989.** IAWA List of microscopic features for hardwood identification. *IAWA Bull. n.s.* **10**: 219–332.
- Isnard S, Silk WK. 2009.** Moving with climbing plants from Charles Darwin’s time into the 21st century. *American Journal of Botany* **96**: 1205-1221.
- Janssen TA, Holtta T, Fleischer K, Naudts K, Dolman H. 2020.** Wood allocation trade-offs between fiber wall, fiber lumen, and axial parenchyma drive drought resistance in neotropical trees. *Plant, cell & environment* **43**: 965-980.
- Johnson D, Eckart P, Alsamadisi N, Noble H, Martin C, Spicer R. 2018.** Polar auxin transport is implicated in vessel differentiation and spatial patterning during secondary growth in *Populus*. *American Journal of Botany* **105**: 186-196.
- Kans J. 2018.** Entrez direct: E-utilities on the UNIX command line. In Entrez Programming Utilities Help [Internet]. *National Center for Biotechnology Information (US)*. <https://www.ncbi.nlm.nih.gov/books/NBK179288/>. Published .
- Kim D, Langmead B, Salzberg SL. 2015.** HISAT: a fast spliced aligner with low memory requirements. *Nature methods* **12**:357.
- Ko JH, Han KH, Park S, Yang J. 2004.** Whole-transcriptome profiling revealed plant body weight-induced secondary growth in *Arabidopsis* and its transcription phenotype. *Plant Physiology* **135**: 1069-1083.
- Koops P, Pelsler S, Ignatz M, Klose C, Marrocco-Selden K, Kretsch T. 2011 .** EDL3 is an F-box protein involved in the regulation of abscisic acid signalling in *Arabidopsis thaliana* . *Journal of experimental botany* **62** : 5547-5560.
- Kubo M, Udagawa M, Nishikubo N, Horiguchi G, Yamaguchi M, Ito J, Mimura T, Fukuda H, Demura T. 2005.** Transcription switches for protoxylem and metaxylem vessel formation. *Genes & development* **19**: 1855-1860.
- Kwon Y, Kim JH, Nguyen HN, Jikumaru Y, Kamiya Y, Hong SW, Lee H. 2013 .** A novel *Arabidopsis* MYB-like transcription factor, MYBH, regulates hypocotyl elongation by enhancing auxin accumulation. *Journal of experimental botany* **64**:3911-3922.
- Lee J, Kim H, Park SG, Hwang H, Yoo SI, Bae W, Kim E, Kim J, Lee H, Heo T et al. 2021.** Brassinosteroid-BZR1/2-WAT1 module determines the high level of auxin signalling in vascular cambium during wood formation. *New Phytologist* **230**: 1503-1516.
- Lens F, Sperry JS, Christman MA, Choat B, Rabaey D, Jansen S. 2011.** Testing hypotheses that link wood anatomy to cavitation resistance and hydraulic conductivity in the genus *Acer*. *New Phytologist* **190** :709–723.
- Li S, Lin YJ, Wang P, Zhang B, Li M, Chen S, Shi R, Tunlaya-Anukit S, Liu X, Wang Z et al. 2019.** The AREB1 transcription factor influences histone acetylation to regulate drought responses and tolerance in *Populus trichocarpa* . *Plant Cell* **31**: 663–686.
- Li L, Xu J, Xu ZH, Xue HW. 2005.** Brassinosteroids stimulate plant tropisms through modulation of polar auxin transport in *Brassica* and *Arabidopsis*. *The Plant Cell* **17**: 2738-2753.

- Liu C, Yu H, Rao X, Dixon R. 2021.** Abscisic acid regulated secondary cell-wall formation and lignin deposition in *Arabidopsis thaliana* through phosphorylation of NST1. *Proceedings of the National Academy of Sciences* **118**: e2010911118.
- Lohmann LG, Taylor CM. 2014.** A new generic classification of tribe Bignoniaceae (Bignoniaceae) 1. *Annals of the Missouri Botanical Garden* **99**: 348-489.
- Lorenzo O, Piqueras R, Sanchez-Serrano JJ, Solano R. 2003.** ETHYLENE RESPONSE FACTOR1 integrates signals from ethylene and jasmonate pathways in plant defense. *Plant Cell* **15**: 165–178.
- Lu D, Wang T, Persson S, Mueller-Roeber B, Schippers JH. 2014.** Transcriptional control of ROS homeostasis by KUODA1 regulates cell expansion during leaf development. *Nature communications* **5**: 3767.
- MacMillan CP, Mansfield SD, Stachurski ZH, Evans R, Southerton SG. 2010.** Fasciclin-like arabinogalactan proteins: specialization for stem biomechanics and cell wall architecture in *Arabidopsis* and *Eucalyptus*. *The Plant Journal* **62**: 689-703.
- Makila R, Wybouw B, Smetana O, Vainio L, Sole-Gil A, Lyu M, Ye L, Wang X, Siligato R, Jenness MK *et al.* 2023.** Gibberellins promote polar auxin transport to regulate stem cell fate decisions in cambium. *Nature plants* **9**: 631-644.
- Manni M, Berkeley MR, Seppey M, Simao FA, Zdobnov EM. 2021.** BUSCO update: novel and streamlined workflows along with broader and deeper phylogenetic coverage for scoring of eukaryotic, prokaryotic, and viral genomes. *Molecular biology and evolution* **38** : 4647-4654.
- Mao JL, Miao ZQ, Wang Z, Yu LH, Cai XT, Xiang CB. 2016.** *Arabidopsis* ERF1 mediates cross-talk between ethylene and auxin biosynthesis during primary root elongation by regulating ASA1 expression. *PLoS genetics* **12**: e1005760.
- Matsumoto-Kitano M, Kusumoto T, Tarkowski P, Kinoshita-Tsujimura K, Vaclavikova K, Miyawaki K, Kakimoto T. 2008.** Cytokinins are central regulators of cambial activity. *Proceedings of the National Academy of Sciences* **105**: 20027-20031.
- Mazur E, Benkova E, Friml J. 2016.** Vascular cambium regeneration and vessel formation in wounded inflorescence stems of *Arabidopsis*. *Scientific reports* **6**: 33754.
- Mazur E, Kurczykńska EU, Friml J. 2014.** Cellular events during interfascicular cambium ontogenesis in inflorescence stems of *Arabidopsis*. *Protoplasma* **251**: 1125-1139.
- Melder E., Bossinger G, Spokevicius AV. 2015.** Overexpression of ARBORKNOX1 delays the differentiation of induced somatic sector analysis (ISSA) derived xylem fibre cells in poplar stems. *Tree Genetics & Genomes* **11**: 1-8.
- Ménard L, McKey D, Rowe N. 2009.** Developmental plasticity and biomechanics of treelets and lianas in *Manihot* aff. *uniquipartite* (Euphorbiaceae): a branch-angle climber of French Guiana. *Annals of Botany* **103**:1249-1259.
- Mrad A, Johnson DM, Love DM, Domec JC. 2021.** The roles of conduit redundancy and connectivity in xylem hydraulic functions. *New Phytologist* **231**: 996-1007.
- Muñiz L, Minguet EG, Singh SK, Pesquet E, Vera-Sirera F, Moreau-Courtois CL, Carbonell J, Blázquez MA, Tuominen H. 2008.** ACAULIS5 controls *Arabidopsis* xylem specification through the prevention of premature cell death. *Development* **135**: 2573-2582.
- Nakajima K, Furutani I, Tachimoto H, Matsubara H, Hashimoto T. 2004.** SPIRAL1 encodes a plant-specific microtubule-localized protein required for directional control of rapidly expanding *Arabidopsis* cells. *The Plant Cell* **16**: 1178-1190.

- Nieminen K, Immanen J, Laxell M, Kauppinen L, Tarkowski P, Dolezal K, Tahtiharju S, Eloa A, Decourteixa M, Ljung K *et al.* 2008. Cytokinin signaling regulates cambial development in poplar. *Proceedings of the National Academy of Sciences* **105**: 20032-20037.
- Novitskaya LL, Tarelkina TV, Galibina NA, Moshchenskaya YL, Nikolaeva NN, Nikerova KM, Podgornaya MN, Sofronova IN, Semenova LI. 2020. The formation of structural abnormalities in Karelian birch wood is associated with auxin inactivation and disrupted basipetal auxin transport. *Journal of Plant Growth Regulation* **39**:378-394.
- Obaton M. 1960. Les Lianes ligneuses à structure anormale des forêts denses d’Afrique occidentale. *Annales des Sciences Naturelles Botanique et Biologie Végétale* **12**: 1–20.
- Pace MR, Lohmann LG, Olmstead RG, Angyalossy V. 2015. Wood anatomy of major Bignoniaceae clades. *Plant Systematics and Evolution* **301**: 967-995.
- Park MY, Kim SA, Lee SJ, Kim SY. 2013. ATHB17 is a positive regulator of abscisic acid response during early seedling growth. *Molecules and Cells* **35**: 125-133.
- Patro R, Duggal G, Love MI, Irizarry RA, Kingsford C. 2017. Salmon provides fast and bias-aware quantification of transcript expression. *Nature methods* **14**: 417.
- Perry ZD, Saminathan T, Arun A, Vaidya BN, Basu C, Reddy UK, Joshee N. 2021. Transcriptome analysis of cambium tissue of *Paulownia* collected during winter and spring. *Diversity* **13**: 423.
- Poorter L, McDonald I, Alarcón A, Fichtler E, Licona JC, Peña-Claros M, Sterck F, Villegas Z, Sass-Klaassen U. 2010. The importance of wood traits and hydraulic conductance for the performance and life history strategies of 42 rainforest tree species. *New phytologist* **185**: 481-492.
- R Development Core Team. 2016. *R: a language and environment for statistical computing, v.3.3.2*. Vienna, Austria: R foundation for Statistical Computing. URL <http://www.r-project.org>.
- Rajput KS, Gondaliya AD, Moya R. 2021. Structure of the secondary xylem and development of a cambial variant in *Serjania mexicana* (Sapindaceae). *IAWA Journal* **43**: 103-115.
- Richter R, Behringer C, Zourelidou M, Schwechheimer C. 2013. Convergence of auxin and gibberellin signaling on the regulation of the GATA transcription factors GNC and GNL in *Arabidopsis thaliana*. *Proceedings of the National Academy of Sciences* **110**:13192-13197.
- Robinson M, McCarthy D, Chen Y, Smyth GK. 2010. edgeR: differential expression analysis of digital gene expression data. *Bioinformatics* **4**: 206-207.
- Robinson MD, Oshlack A. 2010. A scaling normalization method for differential expression analysis of RNA-seq data. *Genome biology* **11**: 25.
- Robinson MD, Smyth GK. 2008. Small-sample estimation of negative binomial dispersion, with applications to SAGE data. *Biostatistics* **9**: 21–332.
- Robischon M, Du J, Miura E, Groover AT. 2011. The Populus class III HD ZIP, *popREVOLUTA*, influences cambium initiation and patterning of woody stems. *Plant physiology* **155**:1214-1225.
- Rowe NP, Speck T. 1996. Biomechanical characteristics of the ontogeny & growth habit of the tropical liana *Condylocarpon guianense* (Apocynaceae). *International Journal of Plant Sciences* **157**: 406-417.
- Rowe N, Speck T. 2005. Plant growth forms: an ecological and evolutionary perspective. *New phytologist* **166**: 61-72.
- Sachs T. 1981. The control of the patterned differentiation of vascular tissues. In *Advances in botanical research*. San Diego, USA: Academic Press, 151-262.

- Sachs T. 2000.** Integrating cellular and organismic aspects of vascular differentiation. *Plant and cell physiology* **41**:649-656.
- Saez A, Apostolova N, Gonzalez-Guzman M, Gonzalez-Garcia MP, Nicolas C, Lorenzo O, Rodriguez PL. 2004.** Gain-of-function and loss-of-function phenotypes of the protein phosphatase 2C HAB1 reveal its role as a negative regulator of abscisic acid signalling. *The Plant Journal* **37**: 354-369.
- Scarpella E, Marcos D, Friml J, Berleth T. 2006.** Control of leaf vascular patterning by polar auxin transport. *Genes & development* **20**: 1015-1027.
- Schenck H. 1893.** Beitrage zur Biologie und Anatomie der Lianen im Besonderen der in Brasilien einheimischen Arten. In Schimper AFW, ed. *Beitrage zur Anatomie der Lianen: Botanische Mittheilungen aus den Tropen*. Jena, Germany: Verlag von Gustav Fisher.
- Schneider CA, Rasband WS, Eliceiri KW. 2012.** NIH Image to ImageJ: 25 years of image analysis. *Nature methods* **9**:671.
- Scholz A, Klepsch M, Karimi Z, Jansen S. 2013.** How to quantify conduits in wood? *Frontiers in Plant Science* **4**: 56.
- Shi D, Jouannet V, Agusti J, Kaul V, Levitsky V, Sanchez P, Mironova VV, Greb T. 2021.** Tissue-specific transcriptome profiling of the Arabidopsis inflorescence stem reveals local cellular signatures. *The Plant Cell* **33**: 200-223.
- Shi D, Lebovka I, Lopez-Salmeron V, Sanchez P, Greb T. 2019.** Bifacial cambium stem cells generate xylem and phloem during radial plant growth. *Development* **146**: dev171355.
- Smyth DR. 2016.** Helical growth in plant organs: mechanisms and significance. *Development* **143**: 3272-3282.
- Snow R. 1935.** Activation of cambial growth by pure hormones. *New Phytologist* **34**: 347-360.
- Soffiatti P, Fort E, Heinz C, Rowe NP. 2022.** Trellis-forming stems of a tropical liana *Condylocarpon guianense* (Apocynaceae): A plant-made safety net constructed by simple “start-stop” development. *Frontiers in Plant Science* **13**.
- Sterky F, Regan S, Karlsson J, Hertzberg M, Rohde A, Holmberg A, Amini B, Bhalerao R, Larsson M, Villarreal R *et al.* 1998.** Gene discovery in the wood-forming tissues of poplar: analysis of 5,692 expressed sequence tags. *Proceedings of the National Academy of Sciences* **95**: 13330-13335.
- Suer S, Agusti J, Sanchez P, Schwarz M, Greb T. 2011.** WOXA imparts auxin responsiveness to cambium cells in Arabidopsis. *The Plant Cell* **23** : 3247-3259.
- Torrey JG, Loomis RS. 1967.** Auxin-cytokinin control of secondary vascular tissue formation in isolated roots of Raphanus. *American Journal of Botany* **54**: 1098-1106.
- Tyree MT, Davis SD, Cochard H. 1994.** Biophysical perspectives of xylem evolution: is there a tradeoff of hydraulic efficiency for vulnerability to dysfunction? *IAWA journal* **15**: 335-360.
- Tyree MT, Zimmermann MH. 2002.** Hydraulic architecture of whole plants and plant performance. In *Xylem structure and the ascent of sap*. New York, USA: Springer-Verlag Berlin Heidelberg: 175-214.
- Uggla C, Moritz T, Sandberg G, Sundberg B. 1996.** Auxin as a positional signal in pattern formation in plants. *Proceedings of the national academy of sciences* **93** : 9282-9286.
- Van Leene J, Hollunder J, Eeckhout D, Persiau G, Van De Slijke E, Stals H, Van Isterdael G, Verkest A, Neiryneck S, Buffel Y *et al.* 2010.** Targeted interactomics reveals a complex core cell cycle machinery in *Arabidopsis thaliana*. *Molecular systems biology* **6**: 397.

- Vo Phan MS, Keren I, Tran PT, Lapidot M, Citovsky V. 2023.** Arabidopsis LSH10 transcription factor and OTLD1 histone deubiquitinase interact and transcriptionally regulate the same target genes. *Communications Biology* **6**: 58.
- Wang Z, Gerstein M, Snyder M. 2009.** RNA-Seq: a revolutionary tool for transcriptomics. *Nature reviews genetics* **10**:57.
- Wang C, Liu N, Geng Z, Ji M, Wang S, Zhuang Y, Chai G. 2022.** Integrated transcriptome and proteome analysis reveals brassinosteroid-mediated regulation of cambium initiation and patterning in woody stem. *Horticulture research* **9**.
- Wason J, Bouda M, Lee EF, McElrone AJ, Phillips RJ, Shackel KA, Matthews MA, Brodersen C. 2021.** Xylem network connectivity and embolism spread in grapevine (*Vitis vinifera* L.). *Plant Physiology* **186**: 373-387.
- Wheeler JK, Sperry JS, Hacke UG, Hoang N. 2005.** Inter-vessel pitting and cavitation in woody Rosaceae and other vesselled plants: a basis for a safety versus efficiency trade-off in xylem transport. *Plant, Cell & Environment* **28**: 800-812.
- Wilcox H. 1962.** Cambial growth characteristics. In Kozlowski TT, ed. *Tree Growth*. New York, Ronald Press Co. pp. 57-88.
- Willige BC, Isono E, Richter R, Zourelidou M, Schwechheimer C. 2011.** Gibberellin regulates PIN-FORMED abundance and is required for auxin transport-dependent growth and development in *Arabidopsis thaliana*. *Plant Cell* **23**: 2184-2195.
- Xu P, Kong Y, Song D, Huang C, Li X, Li L. 2014.** Conservation and functional influence of alternative splicing in wood formation of *Populus* and *Eucalyptus*. *BMC genomics* **15**: 780.
- Xie J, Li M, Zeng J, Li X, Zhang D. 2022.** Single-cell RNA sequencing profiles of stem-differentiating xylem in poplar. *Plant Biotechnology Journal* **20**: 417.
- Yamamoto R, Demura T, Fukuda H. 1997.** Brassinosteroids induce entry into the final stage of tracheary element differentiation in cultured *Zinnia* cells. *Plant and Cell Physiology* **38**:980-983.
- Yang C, Song J, Ferguson AC, Klisch D, Simpson K, Mo R, Taylor B, Mitsuda N, Wilson ZA. 2017.** Transcription factor MYB26 is key to spatial specificity in anther secondary thickening formation. *Plant physiology* **175**: 333-350.
- Yang C, Xu Z, Song J, Conner K, Barrena GV, Wilson ZA. 2007.** Arabidopsis MYB26/MALE STERILE35 regulates secondary thickening in the endothecium and is essential for anther dehiscence. *The Plant Cell* **19**: 534-548.
- Ye ZH, Zhong R. 2015.** Molecular control of wood formation in trees. *Journal of experimental botany* **66**: 4119-4131.
- Yoshida T, Nishimura N, Kitahata N, Kuromori T, Ito T, Asami T, Shinozaki K, Hirayama T. 2006.** ABA-hypersensitive germination3 encodes a protein phosphatase 2C (AtPP2CA) that strongly regulates abscisic acid signaling during germination among Arabidopsis protein phosphatase 2Cs. *Plant physiology* **140**: 115-126.
- Yu D, Janz D, Zienkiewicz K, Herrfurth C, Feussner I, Chen S, Polle A. 2021.** Wood formation under severe drought invokes adjustment of the hormonal and transcriptional landscape in Poplar. *International Journal of Molecular Sciences* **22**: 9899.
- Zhang J, Eswaran G, Alonso-Serra J, Kucukoglu M, Xiang J, Yang W, Elo A, Nieminen K, Damen T, Joung J *et al.* 2019.** Transcriptional regulatory framework for vascular cambium development in Arabidopsis roots. *Nature plants* **5**: 1033-1042.

**Zhang Q, Luo F, Zhong Y, He J, Li L. 2020.** Modulation of NAC transcription factor NST1 activity by XYLEM NAC DOMAIN1 regulates secondary cell wall formation in Arabidopsis. *Journal of experimental botany* **71**:1449-1458.

**Zhbannikov IY, Hunter SS, Foster JA, Settles ML. 2017.**SeqyClean: a pipeline for high-throughput sequence data preprocessing. In *Proceedings of the 8th ACM International Conference on Bioinformatics, Computational Biology, and Health Informatics*: 407-416.

**Zhong R, Demura T, Ye ZH. 2006.** *SND1*, a NAC domain transcription factor, is a key regulator of secondary wall synthesis in fibers of Arabidopsis. *The Plant Cell* **18** : 3158-3170.

**Zhong R, Kandasamy MK, Ye ZH. 2021.** XND1 regulates secondary wall deposition in xylem vessels through the inhibition of VND functions. *Plant and Cell Physiology* **62**: 53-65.

**Zhong R, Lee C, McCarthy RL, Reeves CK, Jones EG, Ye ZH. 2011.** Transcriptional activation of secondary wall biosynthesis by rice and maize NAC and MYB transcription factors. *Plant and Cell Physiology* **52**: 1856-1871.

**Zhong R, Richardson EA, Ye ZH. 2007.** The MYB46 transcription factor is a direct target of SND1 and regulates secondary wall biosynthesis in Arabidopsis. *Plant Cell* **19**: 2776–2792.

**Ziemińska K, Westoby M, Wright IJ. 2015.** Broad anatomical variation within a narrow wood density range—a study of twig wood across 69 Australian angiosperms. *PLoS One* **10**: e0124892.

**Zimmermann MH, Jeje AA. 1981.** Vessel-length distribution in stems of some American woody plants. *Canadian Journal of Botany* **59**: 1882-1892.

**Zinkgraf M, Gerttula S, Groover A. 2017.** Transcript profiling of a novel plant meristem, the monocot cambium. *Journal of integrative plant biology* **59** : 436-449.

## Supporting Information

**Supporting Information Fig. S1.** *B. magnifica* cambium activity and secondary xylem production assessment.

**Supporting Information Fig. S2.** Schematic representation of *B. magnifica* stem segment for RNA sampling.

**Supporting Information Fig. S3.** RNA-seq experiment workflow.

**Supporting Information Fig. S4.** *B. magnifica* exclusive Biological Processes GO terms.

**Supporting Information Fig. S5.** Expression profiles multidimensional scaling plot (MDS).

**Supporting Information Table S1.** *B. magnifica* biological samples sequencing data, annotated transcripts, associated GO terms, and read counts.

**Supporting Information Table S2.** Comparison between GO terms numbers of *B. magnifica* and model trees *Populus x euroamericana* and *Eucalyptus grandis*

**Supporting Information Table S3.** *B. magnifica* differentially expressed genes (DEGs) and category enrichment analysis.

**Supporting Information Table S4.** *B. magnifica* DEGs hand-curated categories.